

SANDIA REPORT

SAND98-2474

Unlimited Release

Printed November 1998

Elastic Wave Radiation from a Line Source of Finite Length

David F. Aldridge

Prepared by
Sandia National Laboratories
Albuquerque, New Mexico 87185 and Livermore, California 94550

Sandia is a multiprogram laboratory operated by Sandia Corporation,
a Lockheed Martin Company, for the United States Department of
Energy under Contract DE-AC04-94AL85000.

Approved for public release; further dissemination unlimited.



Sandia National Laboratories

Issued by Sandia National Laboratories, operated for the United States Department of Energy by Sandia Corporation.

NOTICE: This report was prepared as an account of work sponsored by an agency of the United States Government. Neither the United States Government nor any agency thereof, nor any of their employees, nor any of their contractors, subcontractors, or their employees, makes any warranty, express or implied, or assumes any legal liability or responsibility for the accuracy, completeness, or usefulness of any information, apparatus, product, or process disclosed, or represents that its use would not infringe privately owned rights. Reference herein to any specific commercial product, process, or service by trade name, trademark, manufacturer, or otherwise, does not necessarily constitute or imply its endorsement, recommendation, or favoring by the United States Government, any agency thereof, or any of their contractors or subcontractors. The views and opinions expressed herein do not necessarily state or reflect those of the United States Government, any agency thereof, or any of their contractors.

Printed in the United States of America. This report has been reproduced directly from the best available copy.

Available to DOE and DOE contractors from
Office of Scientific and Technical Information
P.O. Box 62
Oak Ridge, TN 37831

Prices available from (615) 576-8401, FTS 626-8401

Available to the public from
National Technical Information Service
U.S. Department of Commerce
5285 Port Royal Rd
Springfield, VA 22161

NTIS price codes
Printed copy: A04
Microfiche copy: A01



SAND98-2474
Unlimited Release
Printed November 1998

ELASTIC WAVE RADIATION FROM A LINE SOURCE OF FINITE LENGTH

David F. Aldridge
Geophysical Technology Department
Sandia National Laboratories
P.O. Box 5800
Albuquerque, New Mexico, 87185-0750

ABSTRACT

Straightforward algebraic expressions describing the elastic wavefield produced by a line source of finite length are derived in circular cylindrical coordinates. The surrounding elastic medium is assumed to be both homogeneous and isotropic, and the source stress distribution is considered axisymmetric. The time- and space-domain formulae are accurate at all distances and directions from the source; no far-field or long-wavelength assumptions are adopted for the derivation. The mathematics yield a unified treatment of three different types of sources: an axial torque, an axial force, and a radial pressure. The torque source radiates only azimuthally polarized shear waves, whereas force and pressure sources generate simultaneous compressional and shear radiation polarized in planes containing the line source. The formulae reduce to more familiar expressions in the two limiting cases where the length of the line source approaches zero and infinity. Far-field approximations to the exact equations indicate that waves radiated parallel to the line source axis are attenuated relative to those radiated normal to the axis. The attenuation is more severe for higher frequencies and for lower wavespeeds. Hence, shear waves are affected more than compressional waves. This frequency- and direction-dependent attenuation is characterized by an extremely simple mathematical formula, and is readily apparent in example synthetic seismograms.

CONTENTS

1.0 Introduction	1
2.0 Derivation	4
3.0 General Wavefield Characteristics	9
3.1 Velocity and Displacement Wavefields	
3.2 P and S Wavefields	
3.3 Point Source Wavefields	
3.4 Infinite Line Source Wavefields	
3.5 Pressure Wavefield	
3.6 Traveltime Function	
4.0 Exact Wavefield Formulae	16
4.1 Torque Source	
4.2 Force Source	
4.3 Pressure Source	
5.0 Far-Field Approximations	21
5.1 Torque Source	
5.2 Force Source	
5.3 Pressure Source	
5.4 Far-Field Directional Filter	
6.0 Numerical Examples	27
7.0 References	30
8.0 Appendices	31
8.1 Appendix A: Cylindrical Coordinate Elastodynamic Solutions	
8.2 Appendix B: Stress Boundary Conditions	
8.3 Appendix C: Limiting Forms of the Zeroth-Order Coefficients	
8.4 Appendix D: Evaluation of a Two-Dimensional Fourier Transform	
8.5 Appendix E: Partial Derivatives	
8.6 Appendix F: Direction-Dependent Wavelet	
8.7 Appendix G: Point Source Wavefields	
8.7.1 Unidirectional Torque	
8.7.2 Unidirectional Force	
8.7.3 Ring Pressure	
9.0 Figures	53

1.0 INTRODUCTION

Elastic wavefields generated by spatially extended sources are of interest in contexts such as seismic exploration, earthquake seismology, borehole seismology, mine blasting, and underground nuclear explosion phenomenology. However, exact algebraic expressions describing the radiated elastic waves are available only for very few extended sources, even when the surrounding medium is assumed to be both homogeneous and isotropic. One example is the spherical cavity subject to uniform interior pressure loading. Another example is the infinite-length line source. The current work is concerned with a *finite*-length line source of elastic waves, and demonstrates that the radiated wavefield can also be characterized by simple time- and space-domain formulae.

The elastic wavefield produced by a line source of finite length h may be obtained from the corresponding wavefield radiated from a point source via a straightforward spatial convolution operation. This property is derived and demonstrated in circular cylindrical coordinates (r, θ, z) , with the line source located in the interval $[-h/2, +h/2]$ on the z -axis. Axisymmetric (i.e., independent of θ) source performance is assumed. Let subscripts “line” and “point” refer to the wavefields generated by line and point sources of the same physical type, respectively. Then, particle displacement vectors generated by each source are related via

$$\mathbf{u}(r, z, t)|_{\text{line}} = \frac{1}{h} \Pi\left(\frac{z}{h}\right) * \mathbf{u}(r, z, t)|_{\text{point}},$$

where $\Pi(x)$ is the rectangle function of unit height and area, and the asterisk denotes convolution with respect to the independent variable z . Convolution with a rectangle function corresponds to averaging. Hence, the line source displacement at coordinate z is the average value, over a spatial aperture of length h centered at z , of the point source displacement. This expression is valid at all distances and directions from the line source, and for source functions with arbitrary time variation; no far-field or long-wavelength approximations are adopted. In the limiting case where the source length h vanishes, the quantity $(1/h)\Pi(z/h)$ approaches a Dirac delta function $\delta(z)$. Then, the above relation implies that the line source displacement reduces to the point source displacement, as expected.

The above expression is derived by solving the elastodynamic equations for a homogeneous and isotropic wholespace in cylindrical (r, θ, z) coordinates. Several investigators (e.g., Heelan, 1953; Jordan, 1962; Abo-Zena, 1977) have solved these equations, assuming an axisymmetric prescribed-stress boundary condition on the interior wall of a circular borehole with radius a . The solution technique involves Fourier transforming field variables and boundary conditions over the axial coordinate z and time t . An exact solution exists in the two-dimensional transformed domain. However, inverting the transform domain solution to obtain time- and space-domain expressions for the elastic wavefield has proved to be difficult. Approximate results have been achieved by assuming i) the observation point is far from the finite-length cylindrical source, and ii) the wavelengths of radiation generated by the source are large with respect to the source dimensions a and h . These assumptions enable the Fourier inversion integrals to be evaluated approximately via asymptotic techniques such as the stationary phase method. Alternately, a purely numerical inversion can be effected.

The present work demonstrates that a mathematically *exact* inversion of the two-dimensional Fourier transformed solution can be obtained in the case where the borehole radius a vanishes. Hence, the results correspond to the elastic wavefield radiated from a line source of finite length. The time and space

domain formulae contain all near-field, intermediate-field, and far-field terms, and are valid for general sourcing functions.

Following Heelan (1953), three distinct source stress distributions are considered. Stresses applied to the borehole wall may act in the radial (r), axial (z), or azimuthal (θ) directions, either individually or in concert. Each source stress is uniformly applied over a finite length h of the borehole wall, and is independent of the azimuthal angle θ . This axisymmetric assumption leads to greatly simplified mathematical analysis, and also constitutes a reasonable approximation for many practical elastic wave sources. In the sequel, the three source stress types given above are referred to as pressure, force, and torque sources, respectively. As the borehole radius a approaches zero, the magnitudes of the applied stresses must increase without bound in order to generate finite (i.e., nonzero) outgoing wavefields. For the pressure and torque sources, the stress \times volume product remains fixed in this limiting process. For the force source, the stress \times surface area product is held constant.

In addition to conceptual appeal, the convolutional relation between point source and line source elastic wavefields has great utilitarian value. A line source wavefield can be easily calculated by numerically evaluating the convolution integral. Expressions describing point source elastic wavefields generated by a unidirectional force, a unidirectional torque, and a ring pressure are required in the convolution integral, and are compiled here in Appendix G. Although the point force and point torque wavefields are reasonably well-known, the exact elastodynamic field radiated from a point pressurized ring source appears to be unknown. This interesting result is a byproduct of the present analysis.

Theoretical expressions for the *far-field* elastic radiation propagated from a line source are obtained simply by expanding the convolution as a power series in the source length h . The far-field formulae entail retaining only those terms in the expansion that are proportional to $1/R$, where R is the source-receiver distance. The far-field approximations reveal that waves radiated parallel to the source axis are attenuated, relative to those radiated in the perpendicular direction. The attenuation is more severe for higher frequencies, and for lower wavespeeds. Hence, shear waves are affected more than compressional waves. Previous formulae purportedly describing far-field waves generated by a finite length cylindrical source (i.e., with nonzero radius a) do *not* contain this frequency- and direction-dependent filtering effect (Heelan, 1953; repeated by White, 1983, pages 206-208). In fact, Heelan's (1953) expressions are identical to the far-field radial and transverse displacement vector components radiated from *point* force, torque, and ring pressure sources. In the course of the analysis, Heelan (1953) appears to have transferred the finite length cylindrical source to a point. Abo-Zena (1977) also makes this criticism, although his formulae are not obviously correct either.

Several investigators concerned with underground nuclear explosions have examined the elastic wavefields generated by explosively loaded, axisymmetric cavities (Glenn et al., 1985, 1986; Rial and Moran, 1986; Glenn and Rial, 1987; Ben-Menahem and Mikhailov, 1995; Gibson et al., 1996). These studies have established both frequency- and direction-dependent attenuation of far-field radial and transverse waves radiated from elongated cylindrical and/or ellipsoidal cavities. A variety of numerical, approximate analytical, and/or heuristic approaches have been employed for the analyses. The line source is probably a reasonable approximation for an axisymmetric cavity with a large aspect ratio (say, greater than 10:1). The present results for the pressurized line source are generally consistent with these earlier results. The current work extends the concept of a frequency- and direction-dependent attenuation filter to force and torque sources, and provides a simple, easily evaluated expression for the filter response.

Two previous attempts to derive the elastic wavefield produced by a finite-length line source approach the problem by considering an elongated ellipsoidal cavity with uniform interior pressure loading (Usami and Hirono, 1956; Hazebroek, 1966). The elastodynamic equations are solved in prolate spheroidal coordinates in the homogeneous and isotropic region exterior to the cavity, subject to a normal-stress boundary condition on the cavity surface. As the minor axes of the ellipsoid are reduced to zero, the radiated wavefield supposedly approaches that generated by a pressurized line source. However, it is extremely difficult to establish the veracity these results, mainly due to the complexity of mathematical analysis in prolate spheroidal coordinates. Hazebroek (1966) asserts that Usami and Hirono (1956) did not apply the stress boundary condition at the ellipsoidal interface correctly. In turn, Hazebroek's (1966) expressions for displacement potential impulse responses are physically inadmissible, because they are unbounded as the time t increases. Eringen and Suhubi (1975, pages 727-734) uncritically repeat Hazebroek's (1966) analysis and conclusions. It should be emphasized that a proper solution of this problem will *not* necessarily reproduce the results obtained herein, because two different limiting situations are considered. The above authors investigate an enclosed ellipsoidal cavity as the transverse dimensions vanish, whereas the present work is concerned with an infinite-length cylindrical borehole with vanishing radius. The cavity is uniformly pressurized, while a normal stress is applied over a *finite* length of the borehole wall. Different elastic wavefields may very well be produced. A resolution of this issue is not attempted here.

2.0 DERIVATION

Consider an infinitely long cylindrical borehole of radius a located in a homogeneous and isotropic elastic wholespace. The elastic medium is characterized by compressional (P) wavespeed α , shear (S) wavespeed β , and mass density ρ . If a time-varying traction is applied to the interior surface of the borehole, then elastic waves are generated that propagate outward into the wholespace with the P-wave and S-wave speeds of the medium. The source stress distribution may also vary spatially over the borehole wall. This problem is amenable to solution in circular cylindrical coordinates (r, θ, z) where the z -coordinate axis coincides with the axis of the borehole. A general solution of the elastodynamic equations in cylindrical coordinates is developed in Appendices A and B. Fortunately, the general solution simplifies considerably in the case where the applied stress does not depend on the azimuth angle θ . This axisymmetric situation is the subject of the current investigation.

Let the radial (r), azimuthal (θ), and axial (z) components of the source stress vector applied to the borehole wall at $r = a$ be denoted $s_r(z, t)$, $s_\theta(z, t)$, and $s_z(z, t)$, respectively. This stress distribution is considered uniform over the axial coordinate range $z = -h/2$ to $z = +h/2$, and zero elsewhere. Then, the components of the source stress vector are

$$s_r(z, t) = s_r \Pi\left(\frac{z}{h}\right) w_r(t), \quad s_\theta(z, t) = s_\theta \Pi\left(\frac{z}{h}\right) w_\theta(t), \quad s_z(z, t) = s_z \Pi\left(\frac{z}{h}\right) w_z(t),$$

where $\Pi(x)$ is the rectangle function of unit height and area ($\Pi(x) = 1$ for $|x| \leq 1/2$, zero otherwise). In these expressions, s_r , s_θ , and s_z are stress magnitude scalars, and $w_r(t)$, $w_\theta(t)$, and $w_z(t)$ are dimensionless source stress waveforms, normalized to unit maximum absolute amplitude. The solution technique entails performing a two-dimensional Fourier transformation of all field quantities over the variables z and t . The corresponding transform variables are denoted k and ω , respectively. Fourier transforming the above components of the source stress vector yields

$$S_r(k, \omega) = s_r h \text{sinc}\left(\frac{hk}{2\pi}\right) W_r(\omega), \quad S_\theta(k, \omega) = s_\theta h \text{sinc}\left(\frac{hk}{2\pi}\right) W_\theta(\omega),$$

$$S_z(k, \omega) = s_z h \text{sinc}\left(\frac{hk}{2\pi}\right) W_z(\omega),$$

where $\text{sinc}(x) \equiv \sin(\pi x)/(\pi x)$. In the sequel, upper case symbols refer to Fourier transforms (in one- or two-dimensions) of lower case counterparts. Hence, $W(\omega)$ is the frequency spectrum of the time-domain function $w(t)$.

In Appendix A, expressions for the three components of the particle displacement vector are derived in the two-dimensional Fourier transformed domain. For the axisymmetric case, and for $r \geq a$, these are

$$U_r = A_0 k_\alpha R'_0(k_\alpha r) + C_0 i k k_\beta R'_0(k_\beta r),$$

$$U_\theta = -E_0 k_\beta R'_0(k_\beta r),$$

$$U_z = A_0 ik R_0(k_\alpha r) + C_0 \left(\frac{\omega^2}{\beta^2} - k^2 \right) R_0(k_\beta r),$$

where a prime denotes differentiation of a function with respect to its argument. The radial eigenfunction $R_0(x)$ is either a Hankel function or a modified Bessel function, of zeroth order. Compressional and shear radial wavenumbers are defined as

$$k_\alpha = \sqrt{\left| \frac{\omega^2}{\alpha^2} - k^2 \right|}, \quad k_\beta = \sqrt{\left| \frac{\omega^2}{\beta^2} - k^2 \right|},$$

respectively. Finally, coefficients A_0 , E_0 , and C_0 depend on the transform variables k and ω , and are obtained by solving the linear equations

$$\begin{bmatrix} G_{11}(a) & 0 & G_{13}(a) \\ 0 & G_{22}(a) & 0 \\ G_{31}(a) & 0 & G_{33}(a) \end{bmatrix} \begin{bmatrix} A_0 \\ E_0 \\ C_0 \end{bmatrix} = \left(\frac{-ha^2}{\rho\alpha^2} \right) \text{sinc}\left(\frac{hk}{2\pi}\right) \begin{bmatrix} s_r W_r \\ s_\theta W_\theta \\ s_z W_z \end{bmatrix}.$$

Matrix elements $G_{ij}(a)$ are defined in Appendix A. Solving these equations for the three coefficients yields

$$A_0 = \left(\frac{ha^2}{\rho\alpha^2 \Delta} \right) \text{sinc}\left(\frac{hk}{2\pi}\right) [s_z W_z G_{13}(a) - s_r W_r G_{33}(a)],$$

$$E_0 = \left(\frac{-ha^2}{\rho\alpha^2 G_{22}(a)} \right) \text{sinc}\left(\frac{hk}{2\pi}\right) s_\theta W_\theta,$$

$$C_0 = \left(\frac{ha^2}{\rho\alpha^2 \Delta} \right) \text{sinc}\left(\frac{hk}{2\pi}\right) [s_r W_r G_{31}(a) - s_z W_z G_{11}(a)],$$

where Δ is the 2×2 determinant $\Delta = G_{11}(a)G_{33}(a) - G_{31}(a)G_{13}(a)$. Defining the source volume $V = \pi a^2 h$ and the source surface area $A = 2\pi ah$, the coefficients can be expressed as

$$A_0 = \frac{1}{2\pi\rho\alpha^2} \text{sinc}\left(\frac{hk}{2\pi}\right) [(s_z A) W_z f_1 - (s_r V) W_r f_2],$$

$$E_0 = \frac{1}{2\pi\rho\alpha^2} \text{sinc}\left(\frac{hk}{2\pi}\right) [(s_\theta V) W_\theta f_3],$$

$$C_0 = \frac{1}{2\pi\rho\alpha^2} \text{sinc}\left(\frac{hk}{2\pi}\right) [(s_r V) W_r f_4 - (s_z A) W_z f_5],$$

where f_i are factors defined by

$$f_1 = \frac{aG_{13}(a)}{\Delta}, \quad f_2 = \frac{2G_{33}(a)}{\Delta}, \quad f_3 = \frac{-2}{G_{22}(a)}, \quad f_4 = \frac{2G_{31}(a)}{\Delta}, \quad f_5 = \frac{aG_{11}(a)}{\Delta}.$$

The above expressions are exact, for nonzero borehole radius a . Their limiting forms, as the borehole radius vanishes, are desired. In this limiting process, the three stress magnitude scalars s_r , s_θ , and s_z increase without bound, such that the products

$$M_r \equiv s_r V, \quad M_\theta \equiv s_\theta V, \quad F_z \equiv s_z A,$$

remain fixed. The choice of symbols is motivated by the fact that a stress-volume product has dimension moment (force times distance, or energy), whereas a stress-area product has dimension force. The limiting forms, as $a \rightarrow 0$, of the three zeroth-order coefficients A_0 , C_0 , and E_0 are derived in Appendix C. These expressions are substituted into the above equations for the transformed particle displacement components. The equations are written in a manner that facilitates subsequent two-dimensional inverse Fourier transformation. Thus, the radial component equation is:

$$(i\omega)^2 U_r = \text{sinc}\left(\frac{hk}{2\pi}\right) \left[\left(\frac{F_z}{4\pi\rho}\right) \frac{\partial}{\partial r} (ik) [2W_z R_0(k_\alpha r) Y_\alpha - 2W_z R_0(k_\beta r) Y_\beta] \right. \\ \left. + \left(\frac{M_r}{4\pi\rho}\right) \frac{\partial}{\partial r} \left\{ 2(ik)^2 [2W_r R_0(k_\alpha r) Y_\alpha - 2W_r R_0(k_\beta r) Y_\beta] - \frac{(i\omega)^2}{\beta^2} [2W_r R_0(k_\alpha r) Y_\alpha] \right\} \right].$$

The azimuthal component equation is:

$$U_\theta = \text{sinc}\left(\frac{hk}{2\pi}\right) \left(\frac{-M_\theta}{4\pi\rho\beta^2}\right) \frac{\partial}{\partial r} [2W_\theta R_0(k_\beta r) Y_\beta].$$

Finally, the axial component equation is:

$$(i\omega)^2 U_z = \text{sinc}\left(\frac{hk}{2\pi}\right) \left[\left(\frac{F_z}{4\pi\rho}\right) \left\{ (ik)^2 [2W_z R_0(k_\alpha r) Y_\alpha - 2W_z R_0(k_\beta r) Y_\beta] + \frac{(i\omega)^2}{\beta^2} [2W_z R_0(k_\beta r) Y_\beta] \right\} \right. \\ \left. + \left(\frac{M_r}{4\pi\rho}\right) \left\{ 2(ik)^3 [2W_r R_0(k_\alpha r) Y_\alpha - 2W_r R_0(k_\beta r) Y_\beta] - \frac{(ik)(i\omega)^2}{\beta^2} [2W_r R_0(k_\alpha r) Y_\alpha - 4W_r R_0(k_\beta r) Y_\beta] \right\} \right].$$

Y_c (where c is either the P-wave speed α or the S-wave speed β) is a simple function of the transform variables k and ω , and is defined in Appendix C. A two-dimensional inverse Fourier transformation on k and ω can now be applied to each of these equations. Three Fourier transform relations are repeatedly utilized. First

$$\text{sinc}\left(\frac{hk}{2\pi}\right) \leftrightarrow \frac{1}{h} \Pi\left(\frac{z}{h}\right) \delta(t),$$

where the double-headed arrow signifies two-dimensional Fourier transform pairing, and $\delta(t)$ is the Dirac delta function. Second,

$$2WR_0(k_c r)Y_c \leftrightarrow \frac{1}{\sqrt{r^2 + z^2}} w\left(t - \frac{\sqrt{r^2 + z^2}}{c}\right).$$

The validity of this relation is established in Appendix D. Finally,

$$(ik)^m (i\omega)^n F(r, k, \omega) \leftrightarrow \frac{\partial^{m+n}}{\partial z^m \partial t^n} f(r, z, t),$$

where $F(r, k, \omega) \leftrightarrow f(r, z, t)$, and m and n are non-negative integers. This is a straightforward two-dimensional generalization of the well-known derivative theorem of Fourier transform theory. Also, in order to simplify notation, the traveltimes of compressional and shear waves from the coordinate origin to field point (r, z) are denoted as

$$\tau_\alpha = \frac{\sqrt{r^2 + z^2}}{\alpha}, \quad \tau_\beta = \frac{\sqrt{r^2 + z^2}}{\beta},$$

respectively. Applying these Fourier transform results to the above equations yields the following space-time formulae for the three components of elastic particle motion.

Radial component:

$$\begin{aligned} \frac{\partial^2 u_r}{\partial t^2} = & \frac{1}{h} \Pi\left(\frac{z}{h}\right) * \left[\left(\frac{F_z}{4\pi\rho} \right) \frac{\partial^2}{\partial r \partial z} \left[\frac{w_z(t - \tau_\alpha) - w_z(t - \tau_\beta)}{\sqrt{r^2 + z^2}} \right] \right. \\ & \left. + \left(\frac{M_r}{4\pi\rho} \right) \left\{ 2 \frac{\partial^3}{\partial r \partial z^2} \left[\frac{w_r(t - \tau_\alpha) - w_r(t - \tau_\beta)}{\sqrt{r^2 + z^2}} \right] - \frac{1}{\beta^2} \frac{\partial^3}{\partial r \partial t^2} \left[\frac{w_r(t - \tau_\alpha)}{\sqrt{r^2 + z^2}} \right] \right\} \right]. \end{aligned}$$

Azimuthal component:

$$u_\theta = \frac{1}{h} \Pi\left(\frac{z}{h}\right) * \left\{ \left(\frac{-M_\theta}{4\pi\rho\beta^2} \right) \frac{\partial}{\partial r} \left[\frac{w_\theta(t - \tau_\beta)}{\sqrt{r^2 + z^2}} \right] \right\}.$$

Axial component:

$$\frac{\partial^2 u_z}{\partial t^2} = \frac{1}{h} \Pi \left(\frac{z}{h} \right) * \left[\left(\frac{F_z}{4\pi\rho} \right) \left\{ \frac{\partial^2}{\partial z^2} \left[\frac{w_z(t-\tau_\alpha) - w_z(t-\tau_\beta)}{\sqrt{r^2+z^2}} \right] + \frac{1}{\beta^2} \frac{\partial^2}{\partial t^2} \left[\frac{w_z(t-\tau_\beta)}{\sqrt{r^2+z^2}} \right] \right\} \right. \\ \left. + \left(\frac{M_r}{4\pi\rho} \right) \left\{ 2 \frac{\partial^3}{\partial z^3} \left[\frac{w_r(t-\tau_\alpha) - w_r(t-\tau_\beta)}{\sqrt{r^2+z^2}} \right] - \frac{1}{\beta^2} \frac{\partial^3}{\partial z \partial t^2} \left[\frac{w_r(t-\tau_\alpha) - 2w_r(t-\tau_\beta)}{\sqrt{r^2+z^2}} \right] \right\} \right].$$

The asterisk denotes one-dimensional convolution over the z -coordinate. These expressions are the desired results. Evidently, the force source and the pressure source generate simultaneous compressional and shear radiation, polarized in (r,z) planes. The torque source radiates only azimuthally polarized S-waves. The precise dependence of the wavefields on the spatial coordinates r and z can be readily obtained by performing the indicated partial differentiations. Appendix E tabulates formulae for several of the required derivatives. Significant features of these elastic wavefields are discussed in subsequent sections.

3.0 GENERAL WAVEFIELD CHARACTERISTICS

3.1 Velocity and Displacement Wavefields

The foregoing analysis yields the components of the particle acceleration vector in the radial and axial directions. However, these can be integrated with respect to time t to obtain velocity and displacement components, after suitable initial conditions are adopted. For example, the radial velocity component v_r is

$$v_r(t) = v_r(t_0) + \int_{t_0}^t a_r(\tau) d\tau,$$

where $a_r(t) = \partial^2 u_r(t) / \partial t^2$ is the radial acceleration. A second integration yields the radial displacement component:

$$u_r(t) = u_r(t_0) + \int_{t_0}^t v_r(\tau) d\tau = u_r(t_0) + v_r(t_0)(t - t_0) + \int_{t_0}^t \int_{t_0}^{\tau} a_r(s) ds d\tau.$$

Typically, vanishing initial conditions are assumed (i.e., $u_r(t_0) = v_r(t_0) = 0$). Explicit dependence of the field variables on the spatial coordinates r and z is suppressed for notational convenience. Analogous formulae exist for the axial velocity and displacement components.

As an example, consider the particle velocity generated by the force source (i.e., set $M_r = 0$ and $M_\theta = 0$ in the general equations). The second partial derivatives ($\partial^2 / \partial t \partial z$ and $\partial^2 / \partial z^2$) in the expressions for the acceleration components are expanded using the formulae in Appendix E, and the results are integrated in time according to the above procedure. Then, radial and axial components of the particle velocity vector can be put into the forms

$$v_r(r, z, t) - v_r(r, z, t_0) = \frac{1}{h} \Pi\left(\frac{z}{h}\right) * \left(\frac{F_z}{4\pi\rho}\right) [q_r(r, z, t) - q_r(r, z, t_0)],$$

$$v_z(r, z, t) - v_z(r, z, t_0) = \frac{1}{h} \Pi\left(\frac{z}{h}\right) * \left(\frac{F_z}{4\pi\rho}\right) [q_z(r, z, t) - q_z(r, z, t_0)],$$

where quantities q_r and q_z are defined as

$$q_r(r, z, t) = \frac{rz}{(r^2 + z^2)^{3/2}} \left[\frac{w'_z(t - \tau_\alpha)}{\alpha^2} - \frac{w'_z(t - \tau_\beta)}{\beta^2} \right] + \frac{3rz}{(r^2 + z^2)^2} \left[\frac{w_z(t - \tau_\alpha)}{\alpha} - \frac{w_z(t - \tau_\beta)}{\beta} \right]$$

$$+ \frac{3rz}{(r^2 + z^2)^{5/2}} \int_{t - \tau_\beta}^{t - \tau_\alpha} w_z(\tau) d\tau,$$

and

$$q_z(r, z, t) = \frac{1}{(r^2 + z^2)^{3/2}} \left[\frac{z^2 w'_z(t - \tau_\alpha)}{\alpha^2} + \frac{r^2 w'_z(t - \tau_\beta)}{\beta^2} \right] + \frac{(2z^2 - r^2)}{(r^2 + z^2)^2} \left[\frac{w_z(t - \tau_\alpha)}{\alpha} - \frac{w_z(t - \tau_\beta)}{\beta} \right] \\ + \frac{(2z^2 - r^2)}{(r^2 + z^2)^{5/2}} \int_{t - \tau_\beta}^{t - \tau_\alpha} w_z(\tau) d\tau.$$

In the common situation where vanishing initial conditions are specified *and* the source wavelet $w_z(t)$ is causal with respect to time t_0 (i.e., $w_z(t) = 0$ for $t < t_0$), then $v_r(r, z, t_0) = v_z(r, z, t_0) = q_r(r, z, t_0) = q_z(r, z, t_0) = 0$. The above expressions for velocity components reduce to the simpler forms

$$v_r(r, z, t) = \frac{1}{h} \Pi\left(\frac{z}{h}\right) * \left(\frac{F_z}{4\pi\rho}\right) q_r(r, z, t), \quad v_z(r, z, t) = \frac{1}{h} \Pi\left(\frac{z}{h}\right) * \left(\frac{F_z}{4\pi\rho}\right) q_z(r, z, t).$$

Note that both velocity components depend on the source force waveform and its first derivative evaluated at the P-wave and S-wave retarded times ($t - \tau_\alpha$ and $t - \tau_\beta$, respectively), as well as the integral of the source wavelet between these two times. Expressions for the particle acceleration components do not contain this integral term, and thus are somewhat simpler. Hence, the subsequent analysis utilizes the acceleration formulae only.

3.2 P and S Wavefields

The total elastodynamic wavefield radiated from a finite-length line source is readily separated into compressional (propagating with the P-wave speed α) and shear (propagating with the S-wave speed β) parts. Let the superscript ‘‘P’’ designate compressional waves. Then, the radial and axial components of the P-wave particle acceleration vector are given by

$$\frac{\partial^2 u_r^P}{\partial t^2} = \frac{1}{h} \Pi\left(\frac{z}{h}\right) * \frac{\partial}{\partial r} q_\alpha(r, z, t), \quad \frac{\partial^2 u_z^P}{\partial t^2} = \frac{1}{h} \Pi\left(\frac{z}{h}\right) * \frac{\partial}{\partial z} q_\alpha(r, z, t),$$

where

$$q_\alpha(r, z, t) = \frac{F_z}{4\pi\rho} \frac{\partial}{\partial z} \left[\frac{w_z(t - \tau_\alpha)}{\sqrt{r^2 + z^2}} \right] + \frac{M_r}{4\pi\rho} \left(\frac{2\partial^2}{\partial z^2} - \frac{1}{\beta^2} \frac{\partial^2}{\partial t^2} \right) \left[\frac{w_r(t - \tau_\alpha)}{\sqrt{r^2 + z^2}} \right].$$

Interestingly, P-waves radiated from the pressure source depend on the shear wavespeed β . Next, let the superscript ‘‘S’’ refer to the shear wavefield. Utilizing the partial derivative results in Appendix E, the radial and axial S-wave acceleration components are put into the form

$$\frac{\partial^2 u_r^S}{\partial t^2} = -\frac{1}{h} \Pi\left(\frac{z}{h}\right) * \frac{\partial}{\partial z} q_\beta(r, z, t), \quad \frac{\partial^2 u_z^S}{\partial t^2} = \frac{1}{h} \Pi\left(\frac{z}{h}\right) * \left(\frac{\partial}{\partial r} + \frac{1}{r} \right) q_\beta(r, z, t),$$

where

$$q_\beta(r, z, t) = \frac{F_z}{4\pi\rho} \frac{\partial}{\partial r} \left[\frac{w_z(t - \tau_\beta)}{\sqrt{r^2 + z^2}} \right] + \frac{M_r}{4\pi\rho} \frac{2\partial^2}{\partial r \partial z} \left[\frac{w_r(t - \tau_\beta)}{\sqrt{r^2 + z^2}} \right].$$

The azimuthal component of the S-wave acceleration vector is generated solely by the torque source, and is

$$\frac{\partial^2 u_\theta^S}{\partial t^2} = -\frac{1}{h} \Pi\left(\frac{z}{h}\right) * \left\{ \frac{M_\theta}{4\pi\rho\beta^2} \frac{\partial}{\partial r} \left[\frac{w_\theta''(t - \tau_\beta)}{\sqrt{r^2 + z^2}} \right] \right\}.$$

Note that the S-wavefield does not display any dependence on the P-wave speed α .

From the above expressions, it is easily demonstrated that $\mathbf{curl} \mathbf{a}^P = \mathbf{0}$ and $\text{div} \mathbf{a}^S = 0$, where \mathbf{a}^P and \mathbf{a}^S are particle acceleration vectors. Hence, the P-wavefield is irrotational and the S-wavefield is equivoluminal.

3.3 Point Source Wavefields

The equations for elastic particle motions derived in the previous sections involve convolutions (over the z -coordinate) with the rectangle function $(1/h)\Pi(z/h)$. Careful examination reveals that all of these wavefields can be written in the generalized form

$$\text{wavefield}(r, z, t)|_{\text{line}} = \frac{1}{h} \Pi\left(\frac{z}{h}\right) * \text{wavefield}(r, z, t)|_{\text{point}},$$

where subscripts “line” and “point” denote fields generated by line and point sources of identical physical type (torque, force, or pressure), respectively. Convolution with a rectangle function corresponds to averaging. Thus, the line source response at coordinate z is the average value, over a spatial aperture of length h centered at z , of the point source response. This is an intuitively appealing result. As $h \rightarrow 0$, the rectangle $(1/h)\Pi(z/h)$ approaches the Dirac delta function $\delta(z)$, and the above expression reduces to an identity, as expected.

For example, the particle displacement generated by the line torque source of length h can be written as

$$u_\theta(r, z, t)|_{\text{line}} = \frac{1}{h} \Pi\left(\frac{z}{h}\right) * u_\theta(r, z, t)|_{\text{point}},$$

where

$$u_\theta|_{\text{point}} = -\frac{M_\theta}{4\pi\rho\beta^2} \frac{\partial}{\partial r} \left[\frac{w_\theta(t - \tau_\beta)}{\sqrt{r^2 + z^2}} \right].$$

Evaluating the partial derivative with the formula in Appendix E gives

$$u_\theta|_{\text{point}} = \frac{M_\theta r}{4\pi\rho\beta^2} \left[\frac{w_\theta'(t - \tau_\beta)}{\beta(r^2 + z^2)} + \frac{w_\theta(t - \tau_\beta)}{(r^2 + z^2)^{3/2}} \right].$$

This is the cylindrical coordinate representation of the displacement field radiated from a point torque located at the coordinate origin, and with moment oriented in the +z-direction. A more familiar expression for the same (Ben-Menahem and Singh, 1981, p. 225, with a sign error) is obtained by converting to spherical polar coordinates via $r = R \sin\phi$ and $z = R \cos\phi$. This version is given in Appendix G.

Similarly, the radial and axial acceleration components generated by both the *line* force source and the *line* pressure source are written as

$$\left. \frac{\partial^2 u_r(r, z, t)}{\partial t^2} \right|_{\text{line}} = \frac{1}{h} \Pi\left(\frac{z}{h}\right) * \left. \frac{\partial^2 u_r(r, z, t)}{\partial t^2} \right|_{\text{point}}, \quad \left. \frac{\partial^2 u_z(r, z, t)}{\partial t^2} \right|_{\text{line}} = \frac{1}{h} \Pi\left(\frac{z}{h}\right) * \left. \frac{\partial^2 u_z(r, z, t)}{\partial t^2} \right|_{\text{point}}.$$

If these equations are compared with previous formulae, then expressions are obtained for the *point* source accelerations generated by the force source and the pressure source in cylindrical coordinates. Converting these to spherical polar coordinates yield the equations given in Appendix G. The expressions for the point force wavefield are consistent with well known results (Ben-Menahem and Singh, 1981, p. 156). However, the elastodynamic wavefield generated by the point pressure source is relatively unfamiliar. Note that this is *not* identical to the wavefield radiated from a point source of compression (i.e., an explosion), which would generate only outgoing P-waves (see Ben-Menahem and Singh, 1981, p. 223). Rather, the present pressure source is better characterized as a “point ring pressure source”. Recall that it is obtained as the limiting case of a uniform radial stress applied to a finite length of cylindrical borehole wall, as both the radius a and the length h vanish, and the stress magnitude increases without bound. As indicated in Appendix G, this type of source simultaneously radiates both P-waves and S-waves.

3.4 Infinite Line Source Wavefields

As the source length h approaches infinity, cylindrically diverging elastic waves are generated that depend only on the radial coordinate r and time t . All of the above expressions reduce to appropriate forms as the limit $h \rightarrow \infty$ is applied. In this limiting process, the source strength per unit of source length must be held constant. Hence, three linear source magnitude densities are defined as

$$\mathcal{M}_\theta \equiv \frac{M_\theta}{h}, \quad \mathcal{M}_r \equiv \frac{M_r}{h}, \quad \mathcal{F}_z \equiv \frac{F_z}{h}.$$

\mathcal{M}_θ and \mathcal{M}_r have physical dimension moment per length (or force) whereas \mathcal{F}_z has dimension force per length. Also, as $h \rightarrow \infty$, the rectangle function $\Pi(z/h) \rightarrow 1$. Convolution with unity yields the definite integral

$$I(r, t; c) \equiv \lim_{h \rightarrow \infty} \Pi\left(\frac{z}{h}\right) * \left[\frac{w(t - \tau_c)}{\sqrt{r^2 + z^2}} \right] = \int_{-\infty}^{+\infty} \frac{1}{\sqrt{r^2 + x^2}} w\left(t - \frac{\sqrt{r^2 + x^2}}{c}\right) dx.$$

In the following formulae, subscript “inf” denotes wavefields obtained after the limit $h \rightarrow \infty$ is applied to the preceding equations for the elastic particle motion components. For the infinite length torque source

$$u_{\theta}|_{\text{inf}} = \frac{-\mathcal{M}_{\theta}}{4\pi\rho\beta^2} \frac{\partial}{\partial r} I_{\theta}(r, t; \beta).$$

Only azimuthal (θ) component motion is generated. For the infinite length force source

$$u_r|_{\text{inf}} = 0, \quad u_z|_{\text{inf}} = \frac{\mathcal{F}_z}{4\pi\rho\beta^2} I_z(r, t; \beta).$$

Thus, this source generates only axial (z) component motion, propagating with the shear wavespeed β . Finally, for the infinite length pressure source

$$u_r|_{\text{inf}} = \frac{-\mathcal{M}_r}{4\pi\rho\beta^2} \frac{\partial}{\partial r} I_r(r, t; \alpha), \quad u_z|_{\text{inf}} = 0.$$

This source generates only radial (r) component motion, propagating with the compressional wavespeed α . Expressions for definite integral $I(r, t; c)$ and its radial derivative are derived in Appendix D. Substituting these into the above equations yields the following formulae for the particle displacement components radiated from various line sources of infinite length.

Torque source:

$$u_{\theta}|_{\text{inf}} = \frac{\mathcal{M}_{\theta}}{2\pi\rho\beta^2 r} \left[w'_{\theta}(t) * \frac{tH\left(t - \frac{r}{\beta}\right)}{\sqrt{t^2 - \frac{r^2}{\beta^2}}} \right].$$

Force source:

$$u_z|_{\text{inf}} = \frac{\mathcal{F}_z}{2\pi\rho\beta^2} \left[w_z(t) * \frac{H\left(t - \frac{r}{\beta}\right)}{\sqrt{t^2 - \frac{r^2}{\beta^2}}} \right].$$

Pressure source:

$$u_r|_{\text{inf}} = \frac{\mathcal{M}_r}{2\pi\rho\beta^2 r} \left[w'_r(t) * \frac{tH\left(t - \frac{r}{\alpha}\right)}{\sqrt{t^2 - \frac{r^2}{\alpha^2}}} \right].$$

In each equation, $H(t)$ is the Heaviside unit step function, and the asterisk denotes convolution in time. Interestingly, each type of source radiates a distinct elastic displacement component. Moreover, at a fixed radial distance r , the displacement waveforms exhibit the well-known “diffusive” character associated with cylindrically diverging waves. The wavelets possess a decaying, infinitely long tail (even when the source waveform is *finite* duration). The above expression for the axial displacement generated by the infinite force source is consistent with an analogous formula in Aki and Richards (1980,

page 231). Also, in the special case where the source pressure waveform $w_r(t) = H(t)$ (i.e., step loading), then the above equation for $u_{r|inf}$ agrees with an equivalent formula in Eringen and Suhubi (1975, page 661). Both of these formulae are derived via the Cagniard-de Hoop method. The present derivation is far simpler.

3.5 Pressure Wavefield

Acoustic pressure is another observable feature of the wavefield radiated from a source in an elastic medium. The pressure within an elastic solid is defined to be $p = (-1/3)\sigma_{kk}$, where σ_{kk} is the trace of the stress tensor. This evaluates to $p = -K \text{div } \mathbf{u}$, where K is the bulk modulus and \mathbf{u} is the particle displacement vector. Although an expression for pressure could be derived by calculating $\text{div } \mathbf{u}$ from the above cylindrical coordinate components of the displacement vector, it is more easily obtained by two-dimensional inverse Fourier transformation. From Appendix A, the transformed pressure, under conditions of axial symmetry, is

$$P = \rho \left(1 - \frac{4}{3}\gamma^2\right) \omega^2 A_0 R_0(k_\alpha r),$$

where $\gamma = \beta/\alpha$. The dimensionless wavespeed ratio γ ranges from zero to $\sqrt{3}/2 \approx 0.866$ for elastic media (assuming materials with negative Poisson ratio are allowed). Hence, $0 \leq 1 - (4/3)\gamma^2 \leq 1$. Substituting in the limiting form (as $a \rightarrow 0$) for the zeroth-order coefficient A_0 gives

$$P = -\left(1 - \frac{4}{3}\gamma^2\right) \text{sinc}\left(\frac{hk}{4\pi}\right) \left\{ \left(\frac{F_z}{4\pi}\right) (ik) [2W_z R_0(k_\alpha r) Y_\alpha] + \left(\frac{M_r}{4\pi}\right) \left(2(ik)^2 - \frac{(i\omega)^2}{\beta^2}\right) [2W_r R_0(k_\alpha r) Y_\alpha] \right\}.$$

Performing an inverse two-dimensional Fourier transform on k and ω yields

$$p = -\left(1 - \frac{4}{3}\gamma^2\right) \frac{1}{h} \Pi\left(\frac{z}{h}\right) * \left\{ \left(\frac{F_z}{4\pi}\right) \frac{\partial}{\partial z} \left[\frac{w_z(t - \tau_\alpha)}{\sqrt{r^2 + z^2}} \right] + \left(\frac{M_r}{4\pi}\right) \left(\frac{2\partial^2}{\partial z^2} - \frac{1}{\beta^2} \frac{\partial^2}{\partial t^2} \right) \left[\frac{w_r(t - \tau_\alpha)}{\sqrt{r^2 + z^2}} \right] \right\}.$$

Thus, the force source and pressure source each generate an acoustic pressure wavefield that propagates outward with the P-wave speed α . Also, note that there is no explicit dependence of the radiated pressure on the mass density ρ of the elastic medium. Since the torque source generates only S-waves, the radiated pressure field from this source is identically zero.

The pressure radiated from each type of source is easily put into the form

$$p|_{\text{line}} = \frac{1}{h} \Pi\left(\frac{z}{h}\right) * p|_{\text{point}},$$

indicating the relationship between line source and point source wavefields. Appendix G gives expressions for the acoustic pressure generated by both a unidirectional point force and a point ring pressure.

Finally, in the limit as $h \rightarrow \infty$, the acoustic pressure radiated from the line pressure source reduces to

$$p|_{\text{inf}} = \frac{\mathcal{M}_r}{2\pi\beta^2} \left(1 - \frac{4}{3}\gamma^2\right) \left[w_r''(t) * \frac{H\left(t - \frac{r}{\alpha}\right)}{\sqrt{t^2 - \frac{r^2}{\alpha^2}}} \right],$$

where \mathcal{M}_r is the moment per unit length. Using the expression for the radial displacement $u_r|_{\text{inf}}$ from the previous section, it is readily verified that $p|_{\text{inf}} = -K \operatorname{div} \mathbf{u}|_{\text{inf}}$. The pressure radiated from the infinite length force source vanishes, because the outgoing wavefield consists solely of shear waves.

3.6 Traveltime Function

The traveltime of an elastic wave (either compressional or shear) propagating from the source to field point (r,z) can be constructed via simple geometric analysis. Thus

$$T_c(r,z) = \frac{r}{c}, \quad |z| < \frac{h}{2},$$

$$T_c(r,z) = \frac{\sqrt{r^2 + (|z| - h/2)^2}}{c}, \quad |z| > \frac{h}{2},$$

where $c = \alpha$ or $c = \beta$. Figure 1 displays the contoured traveltime field as a function of dimensionless radial and axial coordinates r/h and z/h , respectively. The line source resides in the interval $[-0.5, +0.5]$ on this plot, and traveltime has been normalized by h/c . Heavy contours depict the line source traveltime field and light contours give the point source traveltime function $(1/c)\sqrt{(r^2+z^2)}$, also normalized by h/c . The contour interval equals 0.5. Obviously, the two traveltime fields agree for $z/h = 0$, and the maximum difference between the two (equal to 0.5) is obtained along the line $r/h = 0$.

4.0 EXACT WAVEFIELD FORMULAE

Exact time- and space-domain expressions for the elastodynamic wavefields radiated from the three line sources are presented in this section. The formulae are valid at any distance and direction from the sources. The torque source generates only azimuthal (θ) particle motion. The force and pressure sources radiate axial (z) and radial (r) particle motion, together with acoustic pressure wavefields.

4.1 Torque Source

The particle displacement radiated from the line torque source of length h is

$$u_{\theta} = \left(\frac{-M_{\theta}}{4\pi\rho\beta^2} \right) \frac{1}{h} \Pi\left(\frac{z}{h}\right) * \frac{\partial}{\partial r} \left[\frac{w_{\theta}(t - \tau_{\beta})}{\sqrt{r^2 + z^2}} \right].$$

Since the convolution is with respect to the coordinate z , it can be distributed over the partial derivative with respect to r , giving

$$u_{\theta} = \left(\frac{-M_{\theta}}{4\pi\rho\beta^2 h} \right) \frac{\partial}{\partial r} \left\{ \Pi\left(\frac{z}{h}\right) * \left[\frac{w_{\theta}(t - \tau_{\beta})}{\sqrt{r^2 + z^2}} \right] \right\}.$$

Alternately, the partial derivative can be evaluated with the formula in Appendix E, yielding

$$u_{\theta} = \left(\frac{M_{\theta} r}{4\pi\rho\beta^2 h} \right) \Pi\left(\frac{z}{h}\right) * \left[\frac{w'_{\theta}(t - \tau_{\beta})}{\beta(r^2 + z^2)} + \frac{w_{\theta}(t - \tau_{\beta})}{(r^2 + z^2)^{3/2}} \right].$$

4.2 Force Source

From the original formulae, the radial and axial components of the particle acceleration vector generated by the force source of length h are given by

$$\frac{\partial^2 u_r}{\partial t^2} = \left(\frac{F_z}{4\pi\rho} \right) \frac{1}{h} \Pi\left(\frac{z}{h}\right) * \frac{\partial^2}{\partial r \partial z} \left[\frac{w_z(t - \tau_{\alpha}) - w_z(t - \tau_{\beta})}{\sqrt{r^2 + z^2}} \right],$$

and

$$\frac{\partial^2 u_z}{\partial t^2} = \left(\frac{F_z}{4\pi\rho} \right) \frac{1}{h} \Pi\left(\frac{z}{h}\right) * \left\{ \frac{\partial^2}{\partial z^2} \left[\frac{w_z(t - \tau_{\alpha}) - w_z(t - \tau_{\beta})}{\sqrt{r^2 + z^2}} \right] + \frac{1}{\beta^2} \frac{\partial^2}{\partial t^2} \left[\frac{w_z(t - \tau_{\beta})}{\sqrt{r^2 + z^2}} \right] \right\},$$

respectively. The equations contain convolutions, over the z -coordinate, with the rectangle function $(1/h)\Pi(z/h)$. However, two of these convolutions may be simplified by exploiting the derivative theorem $f(x)*g'(x) = f'(x)*g(x)$, and the fact that the derivative of a rectangle function is a pair of Dirac delta functions with opposing polarities:

$$\frac{\partial}{\partial z} \Pi\left(\frac{z}{h}\right) = \delta\left(z + \frac{h}{2}\right) - \delta\left(z - \frac{h}{2}\right).$$

Thus, the above expressions for the acceleration components are rewritten as

$$\frac{\partial^2 u_r}{\partial t^2} = \left(\frac{F_z}{4\pi\rho h}\right) \left[\delta\left(z + \frac{h}{2}\right) - \delta\left(z - \frac{h}{2}\right) \right] * \frac{\partial}{\partial t} \left[\frac{w_z(t - \tau_\alpha) - w_z(t - \tau_\beta)}{\sqrt{r^2 + z^2}} \right],$$

$$\begin{aligned} \frac{\partial^2 u_z}{\partial t^2} = & \left(\frac{F_z}{4\pi\rho h}\right) \left\{ \left[\delta\left(z + \frac{h}{2}\right) - \delta\left(z - \frac{h}{2}\right) \right] * \frac{\partial}{\partial z} \left[\frac{w_z(t - \tau_\alpha) - w_z(t - \tau_\beta)}{\sqrt{r^2 + z^2}} \right] \right. \\ & \left. + \frac{1}{\beta^2} \Pi\left(\frac{z}{h}\right) * \left[\frac{w_z''(t - \tau_\beta)}{\sqrt{r^2 + z^2}} \right] \right\}. \end{aligned}$$

Convolutions with Dirac delta functions are trivial. Also, expressions for the above partial derivatives are tabulated in Appendix E. In order to simplify notation in subsequent formulae, several definitions are introduced. First, distances from the ends of the line source at $\pm h/2$ to field point (r, z) are designated

$$R_+ = \sqrt{r^2 + (z - h/2)^2}, \quad R_- = \sqrt{r^2 + (z + h/2)^2},$$

respectively. The corresponding traveltimes of P- and S-waves propagating from the ends of the line source to field point (r, z) are

$$\tau_\alpha^+ = \frac{R_+}{\alpha}, \quad \tau_\beta^+ = \frac{R_+}{\beta}, \quad \tau_\alpha^- = \frac{R_-}{\alpha}, \quad \tau_\beta^- = \frac{R_-}{\beta}.$$

Finally, define the functions $q_+(r, z, t)$ and $q_-(r, z, t)$ as the following combination of source waveforms and derivatives:

$$q_\pm(r, z, t) = \frac{w_z'(t - \tau_\alpha^\pm)}{\alpha} - \frac{w_z'(t - \tau_\beta^\pm)}{\beta} + \frac{w_z(t - \tau_\alpha^\pm) - w_z(t - \tau_\beta^\pm)}{R_\pm}.$$

Performing the above convolutions with the Dirac delta functions then yields the following compact expressions for the radial and axial acceleration components:

$$\frac{\partial^2 u_r}{\partial t^2} = \left(\frac{F_z r}{4\pi\rho h}\right) \left[\frac{q_+(r, z, t)}{R_+^2} - \frac{q_-(r, z, t)}{R_-^2} \right],$$

and

$$\frac{\partial^2 u_z}{\partial t^2} = \left(\frac{F_z}{4\pi\rho h}\right) \left\{ \frac{(z - h/2)q_+(r, z, t)}{R_+^2} - \frac{(z + h/2)q_-(r, z, t)}{R_-^2} + \frac{1}{\beta^2} \Pi\left(\frac{z}{h}\right) * \left[\frac{w_z''(t - \tau_\beta)}{\sqrt{r^2 + z^2}} \right] \right\}.$$

The acoustic pressure radiated from the line force source is obtained via the same procedure. From the original expression, this pressure is

$$p = -\left(\frac{F_z}{4\pi}\right)\left(1 - \frac{4}{3}\gamma^2\right)\frac{1}{h}\Pi\left(\frac{z}{h}\right) * \frac{\partial}{\partial z} \left[\frac{w_z(t - \tau_\alpha)}{\sqrt{r^2 + z^2}} \right].$$

Converting the convolution with the rectangle function to convolutions with Dirac delta functions yields

$$p = \left(\frac{F_z}{4\pi h}\right)\left(1 - \frac{4}{3}\gamma^2\right) \left\{ \frac{w_z(t - \tau_\alpha^+)}{R_+} - \frac{w_z(t - \tau_\alpha^-)}{R_-} \right\}.$$

4.3 Pressure Source

Now that notation and methodology are established, the analysis for the line pressure source of length h can proceed quickly. The radial and axial components of the particle acceleration vector generated by this source are

$$\frac{\partial^2 u_r}{\partial t^2} = \left(\frac{M_r}{4\pi\rho}\right)\frac{1}{h}\Pi\left(\frac{z}{h}\right) * \left\{ 2 \frac{\partial^3}{\partial r \partial z^2} \left[\frac{w_r(t - \tau_\alpha) - w_r(t - \tau_\beta)}{\sqrt{r^2 + z^2}} \right] - \frac{1}{\beta^2} \frac{\partial^3}{\partial r \partial t^2} \left[\frac{w_r(t - \tau_\alpha)}{\sqrt{r^2 + z^2}} \right] \right\},$$

and

$$\frac{\partial^2 u_z}{\partial t^2} = \left(\frac{M_r}{4\pi\rho}\right)\frac{1}{h}\Pi\left(\frac{z}{h}\right) * \left\{ 2 \frac{\partial^3}{\partial z^3} \left[\frac{w_r(t - \tau_\alpha) - w_r(t - \tau_\beta)}{\sqrt{r^2 + z^2}} \right] - \frac{1}{\beta^2} \frac{\partial^3}{\partial z \partial t^2} \left[\frac{w_r(t - \tau_\alpha) - 2w_r(t - \tau_\beta)}{\sqrt{r^2 + z^2}} \right] \right\}$$

respectively. Proceeding in a manner identical to the force source, convolutions with the rectangle function can be converted to convolutions with Dirac delta functions. Thus

$$\begin{aligned} \frac{\partial^2 u_r}{\partial t^2} = & \left(\frac{M_r}{4\pi\rho h}\right) \left\{ \left[\delta\left(z + \frac{h}{2}\right) - \delta\left(z - \frac{h}{2}\right) \right] * 2 \frac{\partial^2}{\partial r \partial z} \left[\frac{w_r(t - \tau_\alpha) - w_r(t - \tau_\beta)}{\sqrt{r^2 + z^2}} \right] \right. \\ & \left. - \frac{1}{\beta^2} \Pi\left(\frac{z}{h}\right) * \frac{\partial}{\partial r} \left[\frac{w_r''(t - \tau_\alpha)}{\sqrt{r^2 + z^2}} \right] \right\}, \end{aligned}$$

and

$$\frac{\partial^2 u_z}{\partial t^2} = \left(\frac{M_r}{4\pi\rho h}\right) \left[\delta\left(z + \frac{h}{2}\right) - \delta\left(z - \frac{h}{2}\right) \right] * \left\{ 2 \frac{\partial^2}{\partial z^2} \left[\frac{w_r(t - \tau_\alpha) - w_r(t - \tau_\beta)}{\sqrt{r^2 + z^2}} \right] \right\}$$

$$\frac{1}{\beta^2} \left[\frac{w_r''(t - \tau_\alpha) - 2w_r''(t - \tau_\beta)}{\sqrt{r^2 + z^2}} \right].$$

Utilizing the formulae in Appendix E for the partial derivatives, and performing the convolutions with the Dirac delta functions, yield

$$\frac{\partial^2 u_r}{\partial t^2} = \left(\frac{-M_r}{4\pi\rho h} \right) \left\{ 2r \left[\frac{(z - h/2)p_+(r, z, t)}{R_+^3} - \frac{(z + h/2)p_-(r, z, t)}{R_-^3} \right] + \frac{1}{\beta^2} \Pi\left(\frac{z}{h}\right) * \frac{\partial}{\partial t} \left[\frac{w_r''(t - \tau_\alpha)}{\sqrt{r^2 + z^2}} \right] \right\},$$

and

$$\begin{aligned} \frac{\partial^2 u_z}{\partial t^2} = & \left(\frac{M_r}{4\pi\rho h} \right) \left\{ \frac{1}{R_+^3} \left[r^2 + (1 - 2\gamma^2)(z - h/2)^2 \right] \frac{w_r''(t - \tau_\alpha^+)}{\beta^2} - 2r^2 \frac{w_r''(t - \tau_\beta^+)}{\beta^2} \right] \\ & - \frac{1}{R_-^3} \left[r^2 + (1 - 2\gamma^2)(z + h/2)^2 \right] \frac{w_r''(t - \tau_\alpha^-)}{\beta^2} - 2r^2 \frac{w_r''(t - \tau_\beta^-)}{\beta^2} \right] \\ & + 2[r^2 - 2(z - h/2)^2] \frac{q_+(r, z, t)}{R_+^4} - 2[r^2 - 2(z + h/2)^2] \frac{q_-(r, z, t)}{R_-^4} \left. \right\}, \end{aligned}$$

where functions $p_\pm(r, z, t)$ are defined as

$$p_\pm(r, z, t) = \frac{w_r''(t - \tau_\alpha^\pm)}{\alpha^2} - \frac{w_r''(t - \tau_\beta^\pm)}{\beta^2} + \frac{3w_r'(t - \tau_\alpha^\pm)}{\alpha R_\pm} - \frac{3w_r'(t - \tau_\beta^\pm)}{\beta R_\pm} + \frac{3w_r(t - \tau_\alpha^\pm) - 3w_r(t - \tau_\beta^\pm)}{R_\pm^2}.$$

Functions $q_\pm(r, z, t)$ are defined in the same manner as in the previous section, except the pressure source waveform $w_r(t)$ is used instead of the force source waveform $w_z(t)$, viz:

$$q_\pm(r, z, t) = \frac{w_r'(t - \tau_\alpha^\pm)}{\alpha} - \frac{w_r'(t - \tau_\beta^\pm)}{\beta} + \frac{w_r(t - \tau_\alpha^\pm) - w_r(t - \tau_\beta^\pm)}{R_\pm}.$$

Also, recall that $\gamma = \beta/\alpha$. In the expression for the radial acceleration, the convolution with respect to z may be distributed over the partial differentiation with respect to r , as with the torque source. Finally, the radiated acoustic pressure field is

$$p = -\left(\frac{M_r}{4\pi} \right) \left(1 - \frac{4}{3}\gamma^2 \right) \frac{1}{h} \Pi\left(\frac{z}{h}\right) * \left\{ 2 \frac{\partial^2}{\partial z^2} \left[\frac{w_r(t - \tau_\alpha)}{\sqrt{r^2 + z^2}} \right] - \frac{1}{\beta^2} \frac{\partial^2}{\partial t^2} \left[\frac{w_r(t - \tau_\alpha)}{\sqrt{r^2 + z^2}} \right] \right\},$$

which evaluates to

$$\begin{aligned}
p = & -\left(\frac{M_r}{4\pi h}\right)\left(1 - \frac{4}{3}\gamma^2\right)\left\{\frac{2(z-h/2)}{R_+^2}\left[\frac{w'_r(t-\tau_\alpha^+)}{\alpha} + \frac{w_r(t-\tau_\alpha^+)}{R_+}\right]\right. \\
& - \frac{2(z+h/2)}{R_-^2}\left[\frac{w'_r(t-\tau_\alpha^-)}{\alpha} + \frac{w_r(t-\tau_\alpha^-)}{R_-}\right] \\
& \left. - \frac{1}{\beta^2}\Pi\left(\frac{z}{h}\right)*\left[\frac{w''_r(t-\tau_\alpha)}{\sqrt{r^2+z^2}}\right]\right\}.
\end{aligned}$$

Note that several of the final formulae, for each source type, contain spatial convolutions, over the coordinate z , with the rectangle function. These are retained in the expressions mainly for ease of understanding and numerical evaluation. However, it is also possible to expand the convolutions in various series representations involving elementary functions. Section 5.0 gives one such expansion.

5.0 FAR-FIELD APPROXIMATIONS

The elastodynamic wavefields radiated from the torque, force, and pressure sources of length h entail spatial convolutions of the form

$$\text{wavefield}(r, z, t)|_{\text{line}} = \frac{1}{h} \Pi\left(\frac{z}{h}\right) * \text{wavefield}(r, z, t)|_{\text{point}},$$

where $\Pi(x)$ is the rectangle function of unit height and area. Subscripts “line” and “point” denote wavefields generated by line and point sources of the same physical type, respectively. The wavefields are either particle motion components or acoustic pressure. Evaluating the convolution integral explicitly gives

$$\text{wavefield}(r, z, t)|_{\text{line}} = \frac{1}{h} \int_{-\infty}^{+\infty} \text{wavefield}(r, x, t)|_{\text{point}} \Pi\left(\frac{z-x}{h}\right) dx = \frac{1}{h} \int_{z-h/2}^{z+h/2} \text{wavefield}(r, x, t)|_{\text{point}} dx.$$

Thus, the line source wavefield equals the average value of the point source wavefield over a spatial interval of length h centered at coordinate z . The integrand may be expanded in a Taylor series about the point $x = z$. Hence

$$\text{wavefield}(r, x, t)|_{\text{point}} = \sum_{n=0}^{\infty} \frac{1}{n!} \frac{\partial^n \text{wavefield}(r, x, t)|_{\text{point}}}{\partial x^n} \Big|_{x=z} (x-z)^n.$$

Substituting this series into the integral, and integrating term-by-term gives

$$\text{wavefield}(r, z, t)|_{\text{line}} = \sum_{n=0}^{\infty} \frac{1}{(n+1)!} \frac{\partial^n \text{wavefield}(r, x, t)|_{\text{point}}}{\partial x^n} \Big|_{x=z} \left(\frac{h}{2}\right)^n \left[\frac{1+(-1)^n}{2}\right].$$

The quantity $[1+(-1)^n]/2$ equals unity for even n and vanishes for odd n . Hence, the series reduces to

$$\text{wavefield}(r, z, t)|_{\text{line}} = \sum_{n=0}^{\infty} \frac{1}{(2n+1)!} \frac{\partial^{2n} \text{wavefield}(r, z, t)|_{\text{point}}}{\partial z^{2n}} \left(\frac{h}{2}\right)^{2n}.$$

Note that the first term of the above series is the point source wavefield. Subsequent terms involve even-order partial derivatives of this wavefield with respect to z . There are no obvious general formulae for the high-order partial derivatives of the elastodynamic wavefields. However, all of these wavefields are linear combinations of the function

$$f(r, z, t) = \frac{1}{\sqrt{r^2 + z^2}} w\left(t - \frac{\sqrt{r^2 + z^2}}{c}\right)$$

and/or its partial derivatives with respect to r , z , and t . Here, $w(t)$ stands for one of the source wavelets $w_d(t)$, $w_z(t)$, or $w_r(t)$, and c is either the P-wavespeed α or the S-wavespeed β . As indicated in Appendix

E, far-field approximations for the partial derivatives of function $f(r,z,t)$ are readily obtained. These far-field approximations involve retaining only those terms in the exact formulae that are proportional to $1/R$, where $R = \sqrt{r^2+z^2}$ is the distance from the coordinate origin to field point (r,z) . Hence, far-field approximations for the derivatives of the *point* source elastodynamic wavefields are easily constructed by linear superposition. These, in turn, are substituted into the above series expansion, yielding far-field series approximations for the wavefields radiated from the various *line* sources. The analytical procedure is illustrated below for the torque, force, and pressure sources. Remarkably, each series that arises can be summed to a simple closed-form mathematical expression. Appendix F establishes that

$$\sum_{n=0}^{\infty} \frac{1}{(2n+1)!} \left(\frac{h \cos \varphi}{2c} \right)^{2n} w^{(2n)}(t - \tau_c) = \frac{1}{t_c(\varphi)} \Pi \left(\frac{t}{t_c(\varphi)} \right) * w(t - \tau_c),$$

where $t_c(\varphi) \equiv h|\cos\varphi|/c$, and the convolution is over the common independent variable t . This expression motivates the definition of a *direction-dependent source wavelet*:

$$w(t, \varphi) \equiv \frac{1}{t_c(\varphi)} \Pi \left(\frac{t}{t_c(\varphi)} \right) * w(t).$$

Symbolically, the direction-dependent waveform $w(t, \varphi)$ is distinguished from the isotropic wavelet $w(t)$ via two arguments, rather than one. Hence, the above infinite series sums to the compact form $w(t - \tau_c, \varphi)$.

As demonstrated in Appendix F, the direction-dependent wavelet is a moving average, over a time window of duration $t_c(\varphi)$, of the physical source wavelet. Hence, $w(t, \varphi)$ is a low-pass/high-cut frequency filtered version of $w(t)$. All of the far-field elastodynamic wavefields radiated from the various line sources can be expressed in terms of an appropriate direction-dependent wavelet. The final formulae are obtained merely by replacing the isotropic source wavelet in the far-field *point* source equations by the analogous direction-dependent waveform. This is a highly appealing as well as utilitarian result.

5.1 Torque Source

The even-order partial derivative, with respect to coordinate z , of the azimuthal displacement component is

$$\frac{\partial^{2n}}{\partial z^{2n}} \left\{ u_{\theta} \Big|_{\text{point}} \right\} = \frac{\partial^{2n}}{\partial z^{2n}} \left\{ \left(\frac{-M_{\theta}}{4\pi\rho\beta^2} \right) \frac{\partial}{\partial r} \left[\frac{w_{\theta}(t - \tau_{\beta})}{\sqrt{r^2 + z^2}} \right] \right\} = \left(\frac{-M_{\theta}}{4\pi\rho\beta^2} \right) \frac{\partial^{2n+1}}{\partial r \partial z^{2n}} \left[\frac{w_{\theta}(t - \tau_{\beta})}{\sqrt{r^2 + z^2}} \right].$$

Introducing the far-field approximation for the mixed partial derivative from Appendix E gives

$$\frac{\partial^{2n}}{\partial z^{2n}} \left\{ u_{\theta} \Big|_{\text{point}} \right\} \approx \left(\frac{M_{\theta} \sin \varphi}{4\pi\rho\beta^3 R} \right) \left(\frac{\cos \varphi}{\beta} \right)^{2n} w_{\theta}^{(2n+1)}(t - \tau_{\beta}),$$

where spherical coordinates (R, φ) are used. The approximate equality symbol emphasizes that this relation is valid only at large source-receiver distances R . Substituting this approximation into the series expansion for particle displacement generated by the line torque yields

$$u_\theta|_{\text{line}} \approx \left(\frac{M_\theta \sin \varphi}{4\pi\rho\beta^3 R} \right) \frac{\partial}{\partial t} \sum_{n=0}^{\infty} \frac{1}{(2n+1)!} \left(\frac{h \cos \varphi}{2\beta} \right)^{2n} w_\theta^{(2n)}(t - \tau_\beta).$$

Finally, as indicated above, the series may be summed to obtain the closed-form expression

$$u_\theta \approx \left(\frac{M_\theta \sin \varphi}{4\pi\rho\beta^3 R} \right) \frac{\partial}{\partial t} w_\theta(t - \tau_\beta, \varphi),$$

where subscript “line” has been omitted for convenience. This expression is quite similar to the far-field azimuthal displacement radiated from a *point* torque source (see Appendix G). The only difference is the direction-dependent wavelet $w_\theta(t, \varphi)$ replaces the isotropic source wavelet $w_\theta(t)$ in the equation. The time derivative of the direction-dependent wavelet is given in Appendix F, yielding the alternative form

$$u_\theta \approx \left(\frac{M_\theta \sin \varphi}{4\pi\rho\beta^3 R} \right) \left[\frac{w_\theta(t - \tau_\beta + t_\beta(\varphi)/2) - w_\theta(t - \tau_\beta - t_\beta(\varphi)/2)}{t_\beta(\varphi)} \right].$$

5.2 Force Source

A similar analysis yields the far-field motion components generated by the line force source. Consider the radial acceleration component first. The even-order partial derivative with respect to z is

$$\begin{aligned} \frac{\partial^{2n}}{\partial z^{2n}} \left\{ \frac{\partial^2 u_r}{\partial t^2} \Big|_{\text{point}} \right\} &= \frac{\partial^{2n}}{\partial z^{2n}} \left\{ \left(\frac{F_z}{4\pi\rho} \right) \frac{\partial^2}{\partial r \partial z} \left[\frac{w_z(t - \tau_\alpha) - w_z(t - \tau_\beta)}{\sqrt{r^2 + z^2}} \right] \right\} \\ &= \left(\frac{F_z}{4\pi\rho} \right) \left\{ \frac{\partial^{2n+2}}{\partial r \partial z^{2n+1}} \left[\frac{w_z(t - \tau_\alpha) - w_z(t - \tau_\beta)}{\sqrt{r^2 + z^2}} \right] \right\}. \end{aligned}$$

The mixed partial derivative is approximated by a far-field spherical coordinate expression from Appendix E, yielding

$$\frac{\partial^{2n}}{\partial z^{2n}} \left\{ \frac{\partial^2 u_r}{\partial t^2} \Big|_{\text{point}} \right\} \approx \left(\frac{F_z \sin \varphi \cos \varphi}{4\pi\rho R} \right) \frac{\partial^2}{\partial t^2} \left\{ \left(\frac{\cos \varphi}{\alpha} \right)^{2n} \frac{w_z^{(2n)}(t - \tau_\alpha)}{\alpha^2} - \left(\frac{\cos \varphi}{\beta} \right)^{2n} \frac{w_z^{(2n)}(t - \tau_\beta)}{\beta^2} \right\}.$$

Substituting this into the expansion for the radial acceleration generated by the line source gives the series

$$\frac{\partial^2 u_r}{\partial t^2} \Big|_{\text{line}} \approx \left(\frac{F_z \sin \varphi \cos \varphi}{4\pi\rho R} \right) \frac{\partial^2}{\partial t^2} \sum_{n=0}^{\infty} \frac{1}{(2n+1)!} \left[\left(\frac{h \cos \varphi}{2\alpha} \right)^{2n} \frac{w_z^{(2n)}(t - \tau_\alpha)}{\alpha^2} - \left(\frac{h \cos \varphi}{2\beta} \right)^{2n} \frac{w_z^{(2n)}(t - \tau_\beta)}{\beta^2} \right]$$

which can be summed to a closed-form expression. Also, for consistency with related results, the second partial derivative with respect to time ($\partial^2/\partial t^2$) is omitted from both sides of the equation to yield the far-field radial displacement component

$$u_r \approx \left(\frac{F_z \sin \varphi \cos \varphi}{4\pi\rho R} \right) \left[\frac{w_z(t - \tau_\alpha, \varphi)}{\alpha^2} - \frac{w_z(t - \tau_\beta, \varphi)}{\beta^2} \right].$$

An analogous procedure can be performed with the axial motion component, giving the far-field approximation

$$u_z \approx \left(\frac{F_z}{4\pi\rho R} \right) \left[\cos^2 \varphi \frac{w_z(t - \tau_\alpha, \varphi)}{\alpha^2} + \sin^2 \varphi \frac{w_z(t - \tau_\beta, \varphi)}{\beta^2} \right].$$

Note that each component includes P-wave motion (propagating with speed α) and S-wave motion (propagating with speed β). These two motions are easily uncoupled by calculating radial and transverse components in spherical polar coordinates, which can be obtained via the linear combinations

$$u_R = u_r \sin \varphi + u_z \cos \varphi, \quad u_\varphi = u_r \cos \varphi - u_z \sin \varphi.$$

Thus

$$u_R \approx \left(\frac{F_z \cos \varphi}{4\pi\rho\alpha^2 R} \right) w_z(t - \tau_\alpha, \varphi), \quad u_\varphi \approx \left(\frac{-F_z \sin \varphi}{4\pi\rho\beta^2 R} \right) w_z(t - \tau_\beta, \varphi).$$

Hence, the far-field radial and transverse displacements propagate individually as compressional and shear waves, respectively. The above two expressions have the same form as the far-field displacement components radiated from the *point* force source (see Appendix G), except the direction-dependent wavelet $w_z(t, \varphi)$ replaces the isotropic source wavelet $w_z(t)$.

Finally, by the same procedure, the far-field acoustic pressure is

$$p \approx \left(\frac{F_z \cos \varphi}{4\pi\alpha R} \right) \left(1 - \frac{4}{3} \gamma^2 \right) \frac{\partial}{\partial t} w_z(t - \tau_\alpha, \varphi).$$

Performing the differentiation with respect to time gives an alternate expression that depends explicitly on the physical source wavelet. The time derivative of the direction-dependent wavelet is given in Appendix F, yielding

$$p \approx \left(\frac{F_z \cos \varphi}{4\pi\alpha R} \right) \left(1 - \frac{4}{3} \gamma^2 \right) \left[\frac{w_z(t - \tau_\alpha + t_\alpha(\varphi)/2) - w_z(t - \tau_\alpha - t_\alpha(\varphi)/2)}{t_\alpha(\varphi)} \right].$$

Recall that γ is the dimensionless wavespeed ratio $\gamma = \beta/\alpha$. From the above relations, it is readily inferred that the ratio of far-field acoustic pressure to far-field radial particle velocity is a positive constant:

$$\left. \frac{p}{v_R} \right|_{far} = \rho\alpha \left(1 - \frac{4}{3}\gamma^2 \right).$$

Thus, radial particle velocity and acoustic pressure are in phase at far-field distances from the line source. This is a common feature of elastodynamic wavefields radiated from numerous different types of point sources within a homogeneous and isotropic medium. The current analysis extends this result to a line force source.

5.3 Pressure Source

The same analytical procedure is used to obtain the far-field displacement components radiated from the line pressure source. Mathematical details of the derivations are omitted for brevity. The results are

$$u_r \approx \left(\frac{M_r \sin \varphi}{4\pi\rho R} \right) \frac{\partial}{\partial t} \left[\left(\frac{\alpha^2}{\beta^2} - 2 \cos^2 \varphi \right) \frac{w_r(t - \tau_\alpha, \varphi)}{\alpha^3} + 2 \cos^2 \varphi \frac{w_r(t - \tau_\beta, \varphi)}{\beta^3} \right],$$

and

$$u_z \approx \left(\frac{M_r \cos \varphi}{4\pi\rho R} \right) \frac{\partial}{\partial t} \left[\left(\frac{\alpha^2}{\beta^2} - 2 \cos^2 \varphi \right) \frac{w_r(t - \tau_\alpha, \varphi)}{\alpha^3} - 2 \sin^2 \varphi \frac{w_r(t - \tau_\beta, \varphi)}{\beta^3} \right].$$

Compressional wave and shear wave portions of these wavefields are readily apparent. Combining the above two equations to obtain radial and transverse components in spherical coordinates gives

$$u_R \approx \left(\frac{M_r}{4\pi\rho\alpha^3 R} \right) \left(\frac{\alpha^2}{\beta^2} - 2 \cos^2 \varphi \right) \frac{\partial}{\partial t} w_r(t - \tau_\alpha, \varphi),$$

$$u_\varphi \approx \left(\frac{M_r \sin 2\varphi}{4\pi\rho\beta^3 R} \right) \frac{\partial}{\partial t} w_r(t - \tau_\beta, \varphi).$$

As with the line force source, far-field radial and transverse displacements generated by the line pressure source propagate individually as P-waves and S-waves, respectively. Also, far-field displacement components radiated from the *line* source can be obtained from those generated by the *point* source merely by substituting the direction-dependent wavelet for the isotropic source wavelet (see Appendix G for expressions for the elastic wavefields generated by a point ring pressure source). Performing the partial differentiations with respect to time t in all of the above equations gives alternative expressions for the field variables that depend explicitly on the physical source wavelet $w_r(t)$. Finally, the radiated far-field acoustic pressure is

$$p \approx \left(\frac{M_r}{4\pi\alpha^2 R} \right) \left(1 - \frac{4}{3}\gamma^2 \right) \left(\frac{\alpha^2}{\beta^2} - 2 \cos^2 \varphi \right) \frac{\partial^2}{\partial t^2} w_r(t - \tau_\alpha, \varphi).$$

Once again, far-field acoustic pressure is in-phase with far-field radial particle velocity.

5.4 Far-Field Directional Filter

The above formulae indicate that far-field radial and transverse displacement components generated by a line source are related to the corresponding components radiated from a point source (of the same physical type) via the frequency-domain expressions

$$U_R(R, \varphi, \omega)|_{\text{line}} = U_R(R, \varphi, \omega)|_{\text{point}} \operatorname{sinc}\left(\frac{\omega \cos \varphi}{\omega_\alpha}\right),$$

$$U_T(R, \varphi, \omega)|_{\text{line}} = U_T(R, \varphi, \omega)|_{\text{point}} \operatorname{sinc}\left(\frac{\omega \cos \varphi}{\omega_\beta}\right),$$

where $\omega_c \equiv 2\pi c/h$, with $c = \alpha$ or $c = \beta$. Subscripts “R” and “T” refer to radial and transverse components of motion, respectively. For the torque source, the transverse displacement is polarized in the θ direction, whereas for force and pressure sources, it is polarized in the φ direction. The multiplicative filter $\operatorname{sinc}(\omega \cos \varphi / \omega_c)$ characterizes the frequency- and direction-dependent attenuative effects associated with an extended line source of length h . Figure 2 graphs the amplitude response of this filter as a function of dimensionless angular frequency ω/ω_c , and for a range of polar angles φ . The high-cut filtering effect is most severe for the axial propagation direction $\varphi = 0$; the response degenerates to all-pass at $\varphi = \pi/2$. Since $\omega_\beta < \omega_\alpha$, the first notch in the filter amplitude spectrum occurs at a lower angular frequency for S-waves than for P-waves, for a given propagation direction.

Several investigators, using a variety of numerical, approximate analytical, and/or heuristic approaches, have demonstrated frequency- and direction-dependence of far-field radial and transverse elastic waves propagated from explosively loaded, axisymmetric cavities (Glenn, et al., 1985, 1986; Rial and Moran, 1986; Glenn and Rial, 1987; Ben-Menahem and Mikhailov, 1995; Gibson et al., 1996). For cavities with large aspect ratios (i.e., long and thin) their results are broadly consistent with the above results for the pressurized line source. Waves radiated parallel to the long axis are attenuated relative to those radiated in the perpendicular direction. The present work extends the concept of a far-field directional filter to force and torque sources, and provides a simple analytical formula for the filter response.

6.0 NUMERICAL EXAMPLES

The numerical simulations presented in this section are restricted to far-field particle velocity wavefields radiated from either point or line sources, mainly because the requisite formulae are quite simple to implement. Far-field particle velocities depend explicitly on the physical source wavelet $w(t)$, or its first or second derivatives; no convolution integrals need to be evaluated. Also, acoustic pressure traces need not be plotted since, in the far-field, they are merely scaled versions of the radial velocity traces.

The source wavelet used for the numerical examples is a causal, finite-duration pulse given by

$$w(t) = \frac{4}{3\sqrt{3}} \left[\sin\left(\frac{2\pi t}{T}\right) - \frac{1}{2} \sin\left(\frac{4\pi t}{T}\right) \right] \Pi\left(\frac{t}{T} - \frac{1}{2}\right),$$

where T is the wavelet duration. This waveform is antisymmetric about the center point $t = T/2$, and has unit magnitude peaks at $t = T/3$ and $t = 2T/3$. Moreover, $w(t)$ and its first two derivatives are continuous. Thus, elastic particle displacement and velocity components radiated from the force, torque, and pressure sources are guaranteed to be continuous functions of the spatial coordinates and time. The Fourier amplitude spectrum of the source waveform is

$$|W(\omega)| = \left(\frac{4\pi}{3\sqrt{3}\omega_0} \right) \left| \operatorname{sinc}\left(1 + \frac{\omega}{\omega_0}\right) - \operatorname{sinc}\left(1 - \frac{\omega}{\omega_0}\right) + \frac{1}{2} \operatorname{sinc}\left(2 + \frac{\omega}{\omega_0}\right) - \frac{1}{2} \operatorname{sinc}\left(2 - \frac{\omega}{\omega_0}\right) \right|,$$

where $\omega_0 \equiv 2\pi/T$. The main lobe of the spectrum is confined to the angular frequency interval between zeros at $\omega = 0$ and $\omega = 3\omega_0$. Subsequent lobes have very low magnitude. Figure 3 displays $w(t)$ and $|W(\omega)|$ as functions of dimensionless time t/T and dimensionless angular frequency ω/ω_0 , respectively. The duration $T = 10$ ms (corresponding to $3f_0 = 3/T = 300$ Hz) is used for the following examples.

Figures 4, 5, and 6 illustrate far-field elastic particle velocity components radiated from *point* force, torque, and pressure sources, respectively. Traces in each panel depict the radial or transverse velocity component observed at polar angle φ , from $\varphi = 0^\circ$ to $\varphi = 180^\circ$ in 5° increments, at a fixed radius $R = 100$ m from the source. Trace length is 150 milliseconds. Earth model parameters used are $\alpha = 2000$ m/s, $\beta = 1000$ m/s, and $\rho = 2000$ kg/m³. Hence, P-wave and S-wave arrival times are $\tau_\alpha = 50$ ms and $\tau_\beta = 100$ ms, respectively. Formulae for the far-field velocities are readily inferred from the exact point source expressions in Appendix G, and are

Force Source:

$$v_R|_{\text{point}} \approx \left(\frac{F \cos \varphi}{4\pi\rho\alpha^2 R} \right) w'(t - \tau_\alpha), \quad v_\varphi|_{\text{point}} \approx \left(\frac{-F \sin \varphi}{4\pi\rho\beta^2 R} \right) w'(t - \tau_\beta).$$

Torque Source:

$$v_R|_{\text{point}} = 0, \quad v_\theta|_{\text{point}} \approx \left(\frac{M \sin \varphi}{4\pi\rho\beta^3 R} \right) w''(t - \tau_\beta).$$

Pressure Source:

$$v_R|_{\text{point}} \approx \left(\frac{M}{4\pi\rho\alpha^3 R} \right) \left(\frac{\alpha^2}{\beta^2} - 2 \cos^2 \varphi \right) w''(t - \tau_\alpha), \quad v_\varphi|_{\text{point}} \approx \left(\frac{M \sin 2\varphi}{4\pi\rho\beta^3 R} \right) w''(t - \tau_\beta).$$

An equality, rather than an approximation, is used for the radial velocity generated by the torque source, because this relation is exact at all distances R . Source magnitudes M and F equal unity, and the trace deflection scale is identical for all plots.

In the far-field, compressional and shear waves decouple into radial and transverse components of motion, for all three source types. Note that the transverse velocity component radiated from the torque source is polarized in the azimuthal (θ) direction, whereas transverse velocities generated by the force and pressure sources are polar (φ) component motions. The dependence of the various wavefields on polar angle φ is evident. It should be emphasized that these radiation patterns are an attribute of the various *point* sources, and are not an effect of extended source length.

Figures 7, 8, and 9 display far-field particle velocity components radiated from *line* force, torque, and pressure sources with lengths $h = 5$ m, respectively. All other parameters used for calculation and display are identical to those associated with the point source plots. Expressions for line source velocity components are easily inferred from the formulae in the previous section, and are

Force Source:

$$v_R|_{\text{line}} \approx \left(\frac{F \cos \varphi}{4\pi\rho\alpha^2 R} \right) \left[\frac{w(t - \tau_\alpha + t_\alpha(\varphi)/2) - w(t - \tau_\alpha - t_\alpha(\varphi)/2)}{t_\alpha(\varphi)} \right],$$

$$v_\varphi|_{\text{line}} \approx \left(\frac{-F \sin \varphi}{4\pi\rho\beta^2 R} \right) \left[\frac{w(t - \tau_\beta + t_\beta(\varphi)/2) - w(t - \tau_\beta - t_\beta(\varphi)/2)}{t_\beta(\varphi)} \right].$$

Torque Source:

$$v_R|_{\text{line}} = 0, \quad v_\theta|_{\text{line}} \approx \left(\frac{M \sin \varphi}{4\pi\rho\beta^3 R} \right) \left[\frac{w'(t - \tau_\beta + t_\beta(\varphi)/2) - w'(t - \tau_\beta - t_\beta(\varphi)/2)}{t_\beta(\varphi)} \right].$$

Pressure Source:

$$v_R|_{\text{line}} \approx \left(\frac{M}{4\pi\rho\alpha^3 R} \right) \left(\frac{\alpha^2}{\beta^2} - 2 \cos^2 \varphi \right) \left[\frac{w'(t - \tau_\alpha + t_\alpha(\varphi)/2) - w'(t - \tau_\alpha - t_\alpha(\varphi)/2)}{t_\alpha(\varphi)} \right],$$

$$v_\varphi|_{\text{line}} \approx \left(\frac{M \sin 2\varphi}{4\pi\rho\beta^3 R} \right) \left[\frac{w'(t - \tau_\beta + t_\beta(\varphi)/2) - w'(t - \tau_\beta - t_\beta(\varphi)/2)}{t_\beta(\varphi)} \right].$$

Recall that $t_c(\varphi) = h|\cos\varphi|/c$ where $c = \alpha$ or $c = \beta$. The above formulae require modification in the special case $\varphi = \pi/2$, where they reduce to the analogous point source equations. Once again, far-field P and S waves decouple into radial and transverse motions, respectively. The high-cut filtering effect of the extended line source is quite evident, especially for shear waves propagating near the two axial directions $\varphi = 0^\circ$ and $\varphi = 180^\circ$. For S-waves radiated along the polar axis, the first notch in the filter occurs at frequency $f_\beta = \beta/h = 200$ Hz, which is well within the main lobe of the source wavelet's amplitude spectrum. For compressional waves, $f_\alpha = \alpha/h = 400$ Hz. Some diminution of P-wave amplitude is visible on the plots for near-axial propagation directions.

Finally, Figures 10, 11, and 12 depict far-field velocity components radiated from force, torque, and pressures sources of length $h = 10$ m, respectively. Attenuation of amplitudes within a broad range of propagation angles about the axial directions is especially severe.

7.0 REFERENCES

- Abo-Zena, A.M., 1977, Radiation from a finite cylindrical explosive source: *Geophysics*, **42**, 1384-1393.
- Aki, K., and Richards, P.G., 1980, *Quantitative seismology, theory and methods*, volume 1: W.H. Freeman and Company.
- Ben-Menahem, A., and Mikhailov, O., 1995, Multipole radiation of seismic waves from explosions in nonspherical cavities and its applications to signal identification: *Journal of the Acoustical Society of America*, **97**, 2675-2698.
- Ben-Menahem, A., and Singh, S.J., 1981, *Seismic waves and sources*: Springer-Verlag.
- Eringen, A.C., and Suhubi, E.S., 1975, *Elastodynamics*, volume 2, linear theory: Academic Press.
- Gibson, Jr., R.L., Toksoz, M.N., and Dong, W., 1996, Seismic radiation from explosively loaded cavities in isotropic and transversely isotropic media: *Bulletin of the Seismological Society of America*, **86**, 1910-1924.
- Glenn, L.A., Ladd, A.J.C., Moran, B., and Wilson, K.A., 1985, Elastic radiation from explosively loaded ellipsoidal cavities in an unbounded medium: *Geophysical Journal of the Royal Astronomical Society*, **81**, 231-241.
- Glenn, L.A., Moran, B., Ladd, A.J.C., Wilson, K.A., and Rial, J.A., 1986, Elastic radiation from explosively-loaded axisymmetric cavities: *Geophysical Journal of the Royal Astronomical Society*, **86**, 119-136.
- Glenn, L.A., and Rial, J.A., 1987, Blast wave effects on decoupling with axisymmetric cavities: *Geophysical Journal of the Royal Astronomical Society*, **91**, 229-239.
- Gradshteyn, I.S., and Ryzhik, I.M., 1994, *Table of integrals, series, and products* (fifth edition): Academic Press.
- Hazebroek, P., 1966, Elastic waves from a finite line source: *Proceedings of the Royal Society of London, Series A*, **294**, 38-65.
- Heelan, P.A., 1953, Radiation from a cylindrical source of finite length: *Geophysics*, **18**, 685-696.
- Jordan, D.W., 1962, The stress wave from a finite, cylindrical explosive source: *Journal of Mathematics and Mechanics*, **11**, 503-551.
- Rial, J.A., and Moran, B., 1986, Radiation patterns for explosively-loaded axisymmetric cavities in an elastic medium: analytic approximations and numerical results: *Geophysical Journal of the Royal Astronomical Society*, **86**, 855-862.
- Usami, T., and Hirono, T., 1956, Elastic waves generated from a spheroidal (*sic*) cavity whose wall is subjected to normal stress of harmonic type: *Papers in Meteorology and Geophysics*, **7**, 288-321.
- White, J.E., 1983, *Underground sound, application of seismic waves*: Elsevier.

8.1 APPENDIX A: CYLINDRICAL COORDINATE ELASTODYNAMIC SOLUTIONS

In circular cylindrical coordinates (r, θ, z) , the components of the elastic particle displacement vector may be obtained from three displacement potential functions

$$\phi(r, \theta, z, t), \quad \psi(r, \theta, z, t), \quad \chi(r, \theta, z, t),$$

(Eringen and Suhubi, 1975, p. 718-723). Assuming no body forces, these potentials satisfy the three-dimensional scalar wave equations

$$\nabla^2 \phi - \frac{1}{\alpha^2} \frac{\partial^2 \phi}{\partial t^2} = 0, \quad \nabla^2 \psi - \frac{1}{\beta^2} \frac{\partial^2 \psi}{\partial t^2} = 0, \quad \nabla^2 \chi - \frac{1}{\beta^2} \frac{\partial^2 \chi}{\partial t^2} = 0,$$

where α and β are P-wave and S-wave speeds in the elastic medium, respectively. In cylindrical coordinates, the Laplacian operator is given by

$$\nabla^2 = \frac{\partial^2}{\partial r^2} + \frac{1}{r} \frac{\partial}{\partial r} + \frac{1}{r^2} \frac{\partial^2}{\partial \theta^2} + \frac{\partial^2}{\partial z^2}.$$

The three components of the particle displacement vector are expressed in terms of the potential functions as follows:

$$u_r = \frac{\partial \phi}{\partial r} + \frac{1}{r} \frac{\partial \psi}{\partial \theta} + \frac{\partial^2 \chi}{\partial r \partial z}, \quad u_\theta = \frac{1}{r} \frac{\partial \phi}{\partial \theta} - \frac{\partial \psi}{\partial r} + \frac{1}{r} \frac{\partial^2 \chi}{\partial \theta \partial z}, \quad u_z = \frac{\partial \phi}{\partial z} + \frac{\partial^2 \chi}{\partial z^2} - \frac{1}{\beta^2} \frac{\partial^2 \chi}{\partial t^2}.$$

Note that the physical dimension of χ differs from that of ϕ and ψ . A general solution of the above equations is obtained after performing a two-dimensional Fourier transformation over the variables z and t . Definitions of the forward and inverse Fourier transforms utilized here are

$$F(r, \theta, k, \omega) = \int_{-\infty-\infty}^{+\infty+\infty} \int f(r, \theta, z, t) \exp[-i(kz + \omega t)] dz dt,$$

$$f(r, \theta, z, t) = \frac{1}{4\pi^2} \int_{-\infty-\infty}^{+\infty+\infty} \int F(r, \theta, k, \omega) \exp[+i(kz + \omega t)] dk d\omega.$$

In the sequel, upper case symbols designate forward Fourier transforms (either one- or two-dimensional) of lower case counterparts. Transforming the three-dimensional scalar wave equations for the potential functions yields the Helmholtz equations

$$\nabla^2 \Phi + \frac{\omega^2}{\alpha^2} \Phi = 0, \quad \nabla^2 \Psi + \frac{\omega^2}{\beta^2} \Psi = 0, \quad \nabla^2 X + \frac{\omega^2}{\beta^2} X = 0.$$

Solutions of these equations that are 1) single-valued in the azimuthal angle θ , 2) bounded as the radial coordinate $r \rightarrow +\infty$, and 3) outward propagating as angular frequency $\omega \rightarrow \pm\infty$, are

$$\Phi(r, \theta, k, \omega) = \sum_{n=0}^{\infty} [A_n(k, \omega) \cos(n\theta) + D_n(k, \omega) \sin(n\theta)] R_n(k_\alpha r),$$

$$\Psi(r, \theta, k, \omega) = \sum_{n=0}^{\infty} [E_n(k, \omega) \cos(n\theta) + B_n(k, \omega) \sin(n\theta)] R_n(k_\beta r),$$

$$X(r, \theta, k, \omega) = \sum_{n=0}^{\infty} [C_n(k, \omega) \cos(n\theta) + F_n(k, \omega) \sin(n\theta)] R_n(k_\beta r).$$

Radial wavenumbers and radial eigenfunctions contained in these expressions are defined as follows. Let c denote either the P-wave speed α or the S-wave speed β . Then

1) For $(\omega/c)^2 - k^2 > 0$:

$$k_c = \sqrt{\left| \frac{\omega^2}{c^2} - k^2 \right|} \quad \text{and} \quad R_n(x) = J_n(x) - i \operatorname{sgn}(\omega) N_n(x) \equiv H_n(x).$$

2) For $(\omega/c)^2 - k^2 < 0$:

$$k_c = \sqrt{\left| \frac{\omega^2}{c^2} - k^2 \right|} \quad \text{and} \quad R_n(x) = K_n(x).$$

3) For $(\omega/c)^2 - k^2 = 0$:

$$k_c = \frac{1}{a} \quad \text{and} \quad R_n(x) = x^{-n}.$$

$J_n(x)$ and $N_n(x)$ are Bessel and Neumann functions of integer order n , respectively. For $\omega < 0$, $H_n(x)$ is the n^{th} -order Hankel function of the *first* kind, whereas for $\omega > 0$, $H_n(x)$ is the n^{th} -order Hankel function of the *second* kind. Finally, $K_n(x)$ is the modified Bessel function of the third kind, of order n . $K_n(x)$ is also known as the n^{th} -order Basset function or Macdonald function. All of these functions approach zero for large values of the argument x .

Coefficients A_n , B_n , C_n , D_n , E_n , and F_n depend on axial wavenumber k and angular frequency ω , and are determined by specifying boundary conditions on the cylinder wall at $r = a$. These boundary conditions may involve prescribed displacements, stresses, or a combination of each. The particular case where a stress distribution is prescribed is treated in Appendix B.

Fourier transforming the above expressions for the displacement vector components, and substituting in the solutions for the displacement potentials, gives the following series solutions for U_r , U_θ , and U_z :

$$U_r = \sum_{n=0}^{\infty} \left\{ \left[A_n k_\alpha R'_n(k_\alpha r) + B_n \frac{n}{r} R_n(k_\beta r) + C_n i k k_\beta R'_n(k_\beta r) \right] \cos(n\theta) \right. \\ \left. + \left[D_n k_\alpha R'_n(k_\alpha r) - E_n \frac{n}{r} R_n(k_\beta r) + F_n i k k_\beta R'_n(k_\beta r) \right] \sin(n\theta) \right\},$$

$$U_\theta = \sum_{n=0}^{\infty} \left\{ \left[D_n \frac{n}{r} R_n(k_\alpha r) - E_n k_\beta R'_n(k_\beta r) + F_n i k \frac{n}{r} R_n(k_\beta r) \right] \cos(n\theta) \right. \\ \left. - \left[A_n \frac{n}{r} R_n(k_\alpha r) + B_n k_\beta R'_n(k_\beta r) + C_n i k \frac{n}{r} R_n(k_\beta r) \right] \sin(n\theta) \right\},$$

$$U_z = \sum_{n=0}^{\infty} \left\{ \left[A_n i k R_n(k_\alpha r) + C_n \left(\frac{\omega^2}{\beta^2} - k^2 \right) R_n(k_\beta r) \right] \cos(n\theta) \right. \\ \left. + \left[D_n i k R_n(k_\alpha r) + F_n \left(\frac{\omega^2}{\beta^2} - k^2 \right) R_n(k_\beta r) \right] \sin(n\theta) \right\},$$

where a prime denotes differentiation of a function with respect to its argument. The expression for U_z may be simplified somewhat by defining $\varepsilon_\beta \equiv \text{sgn}[(\omega/\beta)^2 - k^2]$. Thus

$$U_z = \sum_{n=0}^{\infty} \left\{ \left[A_n i k R_n(k_\alpha r) + C_n \varepsilon_\beta k_\beta^2 R_n(k_\beta r) \right] \cos(n\theta) \right. \\ \left. + \left[D_n i k R_n(k_\alpha r) + F_n \varepsilon_\beta k_\beta^2 R_n(k_\beta r) \right] \sin(n\theta) \right\}.$$

In order to solve boundary value problems where tractions are prescribed on a cylindrical surface of fixed radius, the stress vector acting on a surface with unit normal in the $+r$ direction is required. This is obtained from the three stress tensor components $\sigma_{rr}(r, \theta, z, t)$, $\sigma_{r\theta}(r, \theta, z, t)$, and $\sigma_{rz}(r, \theta, z, t)$; the remaining stress tensor components are not needed for the analysis. In cylindrical coordinates, these stress tensor components depend on the displacement vector components via

$$\sigma_{rr} = \rho \alpha^2 \frac{\partial u_r}{\partial r} + \rho (\alpha^2 - 2\beta^2) \left[\frac{u_r}{r} + \frac{1}{r} \frac{\partial u_\theta}{\partial \theta} + \frac{\partial u_z}{\partial z} \right],$$

$$\sigma_{r\theta} = \rho \beta^2 \left[\frac{1}{r} \frac{\partial u_r}{\partial \theta} + \frac{\partial u_\theta}{\partial r} - \frac{u_\theta}{r} \right],$$

$$\sigma_{rz} = \rho \beta^2 \left[\frac{\partial u_r}{\partial z} + \frac{\partial u_z}{\partial r} \right],$$

where ρ is the mass density of the elastic medium. Substituting the expressions for the particle displacement components in terms of the potential functions into these equations gives

$$\sigma_{rr} = \rho(1-2\gamma^2) \frac{\partial^2 \phi}{\alpha^2} + 2\rho\beta^2 \left[\frac{\partial^2 \phi}{\alpha^2} + \frac{1}{r} \left(\frac{\partial^2 \psi}{\partial r \partial \theta} - \frac{1}{r} \frac{\partial \psi}{\partial \theta} \right) + \frac{\partial^2 \chi}{\alpha^2 \partial z} \right],$$

$$\sigma_{r\theta} = \rho\beta^2 \left[\frac{2}{r} \left(\frac{\partial^2 \phi}{\partial r \partial \theta} - \frac{1}{r} \frac{\partial \phi}{\partial \theta} \right) - 2 \frac{\partial^2 \psi}{\alpha^2} - \frac{\partial^2 \psi}{\partial z^2} + \frac{1}{\beta^2} \frac{\partial^2 \psi}{\alpha^2} + \frac{2}{r} \left(\frac{\partial^3 \chi}{\partial r \partial \theta \partial z} - \frac{1}{r} \frac{\partial^2 \chi}{\partial \theta \partial z} \right) \right],$$

$$\sigma_{rz} = \rho\beta^2 \left[2 \frac{\partial^2 \phi}{\alpha \partial z} + \frac{1}{r} \frac{\partial^2 \psi}{\partial \theta \partial z} + 2 \frac{\partial^3 \chi}{\alpha \partial z^2} - \frac{1}{\beta^2} \frac{\partial^3 \chi}{\alpha \partial z^2} \right],$$

where $\gamma \equiv \beta/\alpha$. Fourier transforming with respect to the variables z and t yields

$$\Sigma_{rr} = -\rho(1-2\gamma^2)\omega^2 \Phi + 2\rho\beta^2 \left[\frac{\partial^2 \Phi}{\alpha^2} + \frac{1}{r} \left(\frac{\partial^2 \Psi}{\partial r \partial \theta} - \frac{1}{r} \frac{\partial \Psi}{\partial \theta} \right) + ik \frac{\partial^2 X}{\alpha^2} \right],$$

$$\Sigma_{r\theta} = \rho\beta^2 \left[\frac{2}{r} \left(\frac{\partial^2 \Phi}{\partial r \partial \theta} - \frac{1}{r} \frac{\partial \Phi}{\partial \theta} \right) - 2 \frac{\partial^2 \Psi}{\alpha^2} - \left(\frac{\omega^2}{\beta^2} - k^2 \right) \Psi + \frac{2ik}{r} \left(\frac{\partial^2 X}{\partial r \partial \theta} - \frac{1}{r} \frac{\partial X}{\partial \theta} \right) \right],$$

$$\Sigma_{rz} = \rho\beta^2 \left[2ik \frac{\partial \Phi}{\alpha} + \frac{ik}{r} \frac{\partial \Psi}{\partial \theta} + \left(\frac{\omega^2}{\beta^2} - 2k^2 \right) \frac{\partial X}{\alpha} \right].$$

Finally, substituting the series solutions for the transformed potentials Φ , Ψ , and X into the above expressions yields the following solutions for the stress tensor components:

$$\Sigma_{rr} = \frac{\rho\alpha^2}{r^2} \sum_{n=0}^{\infty} \left\{ [G_{11}(r)A_n + G_{12}(r)B_n + G_{13}(r)C_n] \cos(n\theta) \right. \\ \left. + [G_{11}(r)D_n - G_{12}(r)E_n + G_{13}(r)F_n] \sin(n\theta) \right\},$$

$$\Sigma_{r\theta} = \frac{\rho\alpha^2}{r^2} \sum_{n=0}^{\infty} \left\{ [G_{21}(r)A_n + G_{22}(r)B_n + G_{23}(r)C_n] \sin(n\theta) \right. \\ \left. + [-G_{21}(r)D_n + G_{22}(r)E_n - G_{23}(r)F_n] \cos(n\theta) \right\},$$

$$\Sigma_{rz} = \frac{\rho\alpha^2}{r^2} \sum_{n=0}^{\infty} \left\{ [G_{31}(r)A_n + G_{32}(r)B_n + G_{33}(r)C_n] \cos(n\theta) \right. \\ \left. + [G_{31}(r)D_n - G_{32}(r)E_n + G_{33}(r)F_n] \sin(n\theta) \right\}.$$

Matrix elements $G_{ij}(r)$ depend on k , ω , and the index n , in addition to the radius r . They are given by

$$G_{11}(r) = 2\gamma^2 (k_\alpha r)^2 R_n''(k_\alpha r) - (1 - 2\gamma^2) \left(\frac{\omega r}{\alpha}\right)^2 R_n(k_\alpha r),$$

$$G_{12}(r) = 2\gamma^2 n [(k_\beta r) R_n'(k_\beta r) - R_n(k_\beta r)],$$

$$G_{13}(r) = 2\gamma^2 ik (k_\beta r)^2 R_n''(k_\beta r),$$

$$G_{21}(r) = -2\gamma^2 n [(k_\alpha r) R_n'(k_\alpha r) - R_n(k_\alpha r)],$$

$$G_{22}(r) = -\gamma^2 \left[2(k_\beta r)^2 R_n''(k_\beta r) + \left(\frac{\omega^2}{\beta^2} - k^2\right) r^2 R_n(k_\beta r) \right],$$

$$G_{23}(r) = -2\gamma^2 ikn [(k_\beta r) R_n'(k_\beta r) - R_n(k_\beta r)],$$

$$G_{31}(r) = 2\gamma^2 ikr (k_\alpha r) R_n'(k_\alpha r),$$

$$G_{32}(r) = \gamma^2 ikrn R_n(k_\beta r),$$

$$G_{33}(r) = \gamma^2 \left(\frac{\omega^2}{\beta^2} - 2k^2\right) (k_\beta r^2) R_n'(k_\beta r).$$

Diagonal elements G_{11} , G_{22} , and G_{33} can be rewritten by defining $\varepsilon_c \equiv \text{sgn}[(\omega/c)^2 - k^2]$ where $c = \alpha$ or $c = \beta$. Then

$$G_{11}(r) = 2\gamma^2 (k_\alpha r)^2 R_n''(k_\alpha r) - (1 - 2\gamma^2) (\varepsilon_\beta k_\beta^2 + k^2) r^2 R_n(k_\alpha r),$$

$$G_{22}(r) = -\gamma^2 (k_\beta r)^2 [2R_n''(k_\beta r) + \varepsilon_\beta R_n(k_\beta r)],$$

$$G_{33}(r) = \gamma^2 k_\beta (\varepsilon_\beta k_\beta^2 - k^2) r^2 R_n'(k_\beta r).$$

These matrix elements possess two-dimensional Hermitian symmetry in the transform variables k and ω . That is, $G_{ij}(r, -k, -\omega) = G_{ij}(r, k, \omega)^*$ where the asterisk denotes complex conjugation. For $(\omega/c)^2 - k^2 \leq 0$ (where $c = \alpha$ or $c = \beta$), this property follows immediately from the definitions given above, and the fact that the radial eigenfunctions $R_n(x)$ are real-valued. For $(\omega/c)^2 - k^2 > 0$, the relations

$$R_n'(x) = \frac{1}{2} [R_{n-1}(x) - R_{n+1}(x)], \quad R_n''(x) = \frac{1}{4} [R_{n-2}(x) - 2R_n(x) + R_{n+2}(x)],$$

satisfied by Hankel functions can be used to eliminate derivatives from the expressions for the $G_{ij}(r)$. Hermitian symmetry is then readily inferred. The implications of Hermitian symmetry for the solution of the unknown series coefficients A_n through F_n is discussed in Appendix B.

Finally, an expression for the pressure wavefield is developed. In an elastic medium, the acoustic pressure is defined as $p = -K \operatorname{div} \mathbf{u}$, where K is the bulk modulus and \mathbf{u} is the particle displacement vector. Using the cylindrical coordinate representation of the divergence operator, as well as $K = \rho\alpha^2 [1 - (4/3)\gamma^2]$ gives

$$p = -\rho\alpha^2 \left(1 - \frac{4}{3}\gamma^2\right) \left[\frac{\partial u_r}{\partial r} + \frac{u_r}{r} + \frac{1}{r} \frac{\partial u_\theta}{\partial \theta} + \frac{\partial u_z}{\partial z} \right].$$

Substituting in the expressions for the displacement vector components in terms of potential functions gives

$$p = -\rho\alpha^2 \left(1 - \frac{4}{3}\gamma^2\right) \nabla^2 \phi = -\rho \left(1 - \frac{4}{3}\gamma^2\right) \frac{\partial^2 \phi}{\partial z^2}.$$

Thus, acoustic pressure depends only on the compressional potential ϕ , which propagates with the P-wave speed α . Fourier transforming on the variables z and t , and substituting the series expansion in angle θ for the transformed compressional potential Φ yields

$$P = \rho \left(1 - \frac{4}{3}\gamma^2\right) \omega^2 \Phi = \rho \left(1 - \frac{4}{3}\gamma^2\right) \omega^2 \sum_{n=0}^{\infty} [A_n \cos(n\theta) + D_n \sin(n\theta)] R_n(k_\alpha r).$$

8.2 APPENDIX B: STRESS BOUNDARY CONDITIONS

Elastic waves are initiated by time-varying stresses applied to the cylinder wall at radius $r = a$. Let the radial, azimuthal, and axial components of the source stress vector be

$$s_r(\theta, z, t), \quad s_\theta(\theta, z, t), \quad s_z(\theta, z, t),$$

respectively. After two-dimensional Fourier transformation

$$S_r(\theta, k, \omega), \quad S_\theta(\theta, k, \omega), \quad S_z(\theta, k, \omega).$$

These transformed stress vector components may be expanded as Fourier cosine and sine series in the azimuth angle θ :

$$S_r(\theta, k, \omega) = \sum_{n=0}^{\infty} \left[P_n^r(k, \omega) \cos(n\theta) + Q_n^r(k, \omega) \sin(n\theta) \right],$$

$$S_\theta(\theta, k, \omega) = \sum_{n=0}^{\infty} \left[P_n^\theta(k, \omega) \cos(n\theta) + Q_n^\theta(k, \omega) \sin(n\theta) \right],$$

$$S_z(\theta, k, \omega) = \sum_{n=0}^{\infty} \left[P_n^z(k, \omega) \cos(n\theta) + Q_n^z(k, \omega) \sin(n\theta) \right].$$

Coefficients in each series are determined from the orthogonal properties of the trigonometric functions. Thus

$$P_n^r(k, \omega) = \frac{d_n}{\pi} \int_0^{2\pi} S_r(\theta, k, \omega) \cos(n\theta) d\theta, \quad Q_n^r(k, \omega) = \frac{1}{\pi} \int_0^{2\pi} S_r(\theta, k, \omega) \sin(n\theta) d\theta,$$

$$P_n^\theta(k, \omega) = \frac{d_n}{\pi} \int_0^{2\pi} S_\theta(\theta, k, \omega) \cos(n\theta) d\theta, \quad Q_n^\theta(k, \omega) = \frac{1}{\pi} \int_0^{2\pi} S_\theta(\theta, k, \omega) \sin(n\theta) d\theta,$$

$$P_n^z(k, \omega) = \frac{d_n}{\pi} \int_0^{2\pi} S_z(\theta, k, \omega) \cos(n\theta) d\theta, \quad Q_n^z(k, \omega) = \frac{1}{\pi} \int_0^{2\pi} S_z(\theta, k, \omega) \sin(n\theta) d\theta,$$

where $d_n = 1$ for $n > 0$ and $d_0 = 1/2$. Note that for $n = 0$, the sine series coefficients vanish, and the cosine series coefficients reduce to average values, over the angular range 0 to 2π , of the corresponding transformed stress vector components.

The stress boundary condition at $r = a$ is mathematically expressed as

$$\sigma_{rr}(a, \theta, z, t) = -s_r(\theta, z, t), \quad \sigma_{r\theta}(a, \theta, z, t) = -s_\theta(\theta, z, t), \quad \sigma_{rz}(a, \theta, z, t) = -s_z(\theta, z, t).$$

Note the negative signs on the right hand sides of these equations. Fourier transforming on z and t gives

$$\Sigma_{rr}(a, \theta, k, \omega) = -S_r(\theta, k, \omega), \quad \Sigma_{r\theta}(a, \theta, k, \omega) = -S_\theta(\theta, k, \omega), \quad \Sigma_{rz}(a, \theta, k, \omega) = -S_z(\theta, k, \omega).$$

The expressions for the transformed stress tensor components, evaluated at $r = a$, are substituted into the left hand sides of these equations. The Fourier series representations of the transformed source stress vector components are substituted into the right hand sides. Equating individual terms in the infinite sums yields two 3×3 linear algebraic systems that the six unknown coefficients A_n through F_n must satisfy:

$$\begin{bmatrix} G_{11}(a) & G_{12}(a) & G_{13}(a) \\ G_{21}(a) & G_{22}(a) & G_{23}(a) \\ G_{31}(a) & G_{32}(a) & G_{33}(a) \end{bmatrix} \begin{bmatrix} A_n \\ B_n \\ C_n \end{bmatrix} = \frac{-a^2}{\rho\alpha^2} \begin{bmatrix} P_n^r \\ Q_n^\theta \\ P_n^z \end{bmatrix},$$

$$\begin{bmatrix} G_{11}(a) & -G_{12}(a) & G_{13}(a) \\ -G_{21}(a) & G_{22}(a) & -G_{23}(a) \\ G_{31}(a) & -G_{32}(a) & G_{33}(a) \end{bmatrix} \begin{bmatrix} D_n \\ E_n \\ F_n \end{bmatrix} = \frac{-a^2}{\rho\alpha^2} \begin{bmatrix} Q_n^r \\ P_n^\theta \\ Q_n^z \end{bmatrix}.$$

In principle, the cylindrical coordinate elastodynamic solution in the two-dimensional Fourier transformed domain is now complete. The above systems are solved for each applicable index n , and the resulting coefficients are substituted into the series for displacement vector components, stress tensor components, and acoustic pressure developed in Appendix A.

The above linear systems possess the Hermitian symmetry in k and ω required for real-valued displacement, stress, and pressure solutions. In particular, since the components of the source stress vector are inherently real, their two-dimensional Fourier transforms are Hermitian [i.e., $S_r(\theta, k, \omega) = S_r(\theta, k, \omega)^*$ and likewise for S_θ and S_z]. This, in turn, implies that the coefficients $P_n(k, \omega)$ and $Q_n(k, \omega)$ in the Fourier cosine and sine expansions are also Hermitian. Finally, since the matrix elements $G_{ij}(a, k, \omega)$ have been shown previously to be Hermitian, the coefficients $A_n(k, \omega)$ through $F_n(k, \omega)$ obtained by solving the above systems are Hermitian as well. This guarantees that displacement potentials ϕ , ψ , χ , displacement vector components u_r , u_θ , u_z , stress tensor components σ_{rr} , $\sigma_{r\theta}$ and σ_{rz} , and acoustic pressure p are all real-valued functions of the variables z and t .

In the important special case where the source stress vector does not depend on the azimuth angle θ , the above formulae simplify considerably. All Fourier series cosine and sine coefficients vanish for $n > 0$, implying that only the zeroth-order coefficients A_0 through F_0 are required for displacement and stress solutions. When $n = 0$, matrix elements $G_{12}(a)$, $G_{21}(a)$, $G_{23}(a)$, and $G_{32}(a)$ also vanish, and the above linear systems reduce to

$$\begin{bmatrix} G_{11}(a) & G_{13}(a) \\ G_{31}(a) & G_{33}(a) \end{bmatrix} \begin{bmatrix} A_0 \\ C_0 \end{bmatrix} = \frac{-a^2}{\rho\alpha^2} \begin{bmatrix} P_0^r \\ P_0^z \end{bmatrix}, \quad G_{22}(a)E_0 = \frac{-a^2}{\rho\alpha^2} P_0^\theta.$$

Solution is straightforward. The remaining three coefficients B_0 , D_0 , and F_0 are not needed in the zeroth-order expressions for displacements, stresses, and/or pressure.

8.3 APPENDIX C: LIMITING FORMS OF THE ZEROth-ORDER COEFFICIENTS

When the borehole radius a vanishes, the limiting forms of five factors must be determined. These factors are defined as

$$f_1 = \frac{aG_{13}(a)}{\Delta}, \quad f_2 = \frac{2G_{33}(a)}{\Delta}, \quad f_3 = \frac{-2}{G_{22}(a)}, \quad f_4 = \frac{2G_{31}(a)}{\Delta}, \quad f_5 = \frac{aG_{11}(a)}{\Delta},$$

where Δ is the determinant

$$\Delta = G_{11}(a)G_{33}(a) - G_{31}(a)G_{13}(a).$$

The matrix elements $G_{ij}(r)$ are defined in Appendix A. However, the expressions given there contain first and second derivatives of the radial eigenfunctions $R_n(x)$. These derivatives can be eliminated via the relations

$$R'_n(x) = -\frac{1}{2}[R_{n+1}(x) - \varepsilon_c R_{n-1}(x)], \quad R''_n(x) = \frac{1}{4}[R_{n+2}(x) - 2\varepsilon_c R_n(x) + R_{n-2}(x)],$$

which hold for both Hankel functions [$\varepsilon_c = +1$ implying $R_n(x) = H_n(x)$] and modified Bessel functions [$\varepsilon_c = -1$ implying $R_n(x) = K_n(x)$]. Evaluating the relevant matrix elements for $n = 0$ and $r = a$ then yields

$$G_{11}(a) = \gamma^2 (k_\alpha a)^2 [R_2(k_\alpha a) - gR_0(k_\alpha a)],$$

$$G_{22}(a) = -\gamma^2 (k_\beta a)^2 R_2(k_\beta a),$$

$$G_{33}(a) = \gamma^2 a(k^2 - \varepsilon_\beta k_\beta^2)(k_\beta a)R_1(k_\beta a),$$

$$G_{13}(a) = \gamma^2 ik(k_\beta a)^2 [R_2(k_\beta a) - \varepsilon_\beta R_0(k_\beta a)],$$

$$G_{31}(a) = -2\gamma^2 ika(k_\alpha a)R_1(k_\alpha a),$$

where $g \equiv [(1-2\gamma^2)(k/k_\alpha)^2 + \varepsilon_\alpha(1-\gamma^2)]/\gamma^2$. Recall that $\varepsilon_c = \text{sgn}[(\omega/c)^2 - k^2]$ with $c = \alpha$ or $c = \beta$, and $\gamma = \beta/\alpha$.

For the analysis in this Appendix, define two dimensionless arguments $x \equiv k_\alpha a$ and $y \equiv k_\beta a$, where k_α and k_β are radial wavenumbers associated with compressional wave and shear wave propagation, respectively. In the limit of vanishing borehole radius a , each approaches zero, but the ratio x/y remains fixed. In terms of x and y , the five factors f_i become

$$f_1 = \frac{ik[y^2 R_2(y) - \varepsilon_\beta y^2 R_0(y)]}{\gamma^2 \hat{\Delta}(x, y)}, \quad f_2 = \frac{2(k^2 - \varepsilon_\beta k_\beta^2)[yR_1(y)]}{\gamma^2 \hat{\Delta}(x, y)},$$

$$f_3 = \frac{2}{\gamma^2 [y^2 R_2(y)]}, \quad f_4 = \frac{-4ik [xR_1(x)]}{\gamma^2 \hat{\Delta}(x,y)}, \quad f_5 = \frac{[x^2 R_2(x) - gx^2 R_0(x)]}{\gamma^2 \hat{\Delta}(x,y)},$$

where

$$\hat{\Delta}(x,y) = (k^2 - \varepsilon_\beta k_\beta^2) [yR_1(y)] [x^2 R_2(x) - gx^2 R_0(x)] - 2k^2 [xR_1(x)] [y^2 R_2(y) - \varepsilon_\beta y^2 R_0(y)].$$

The quantities in square brackets in the above expressions approach well defined limits as x and y vanish. Consider the situation $\varepsilon_\alpha = +1$ first. In this case, the radial eigenfunctions are Hankel functions of the first or second kind. For small argument x , these low order Hankel functions are approximated as

$$H_0(x) \approx -i \operatorname{sgn}(\omega) \frac{2}{\pi} \ln\left(\frac{x}{2}\right), \quad H_1(x) \approx i \operatorname{sgn}(\omega) \left(\frac{2}{\pi x}\right), \quad H_2(x) \approx i \operatorname{sgn}(\omega) \left(\frac{4}{\pi x^2}\right).$$

Hence

$$\lim_{x \rightarrow 0} x^2 H_0(x) = 0, \quad \lim_{x \rightarrow 0} x H_1(x) = i \operatorname{sgn}(\omega) \frac{2}{\pi}, \quad \lim_{x \rightarrow 0} x^2 H_2(x) = i \operatorname{sgn}(\omega) \frac{4}{\pi}.$$

Next, consider the situation $\varepsilon_\alpha = -1$. The radial eigenfunctions are modified Bessel functions, with small argument approximations

$$K_0(x) \approx \ln\left(\frac{2}{x}\right), \quad K_1(x) \approx \frac{1}{x}, \quad K_2(x) \approx \frac{2}{x^2}.$$

Thus

$$\lim_{x \rightarrow 0} x^2 K_0(x) = 0, \quad \lim_{x \rightarrow 0} x K_1(x) = 1, \quad \lim_{x \rightarrow 0} x^2 K_2(x) = 2.$$

Clearly, *exactly* the same limits hold when the cases $\varepsilon_\beta = \pm 1$ are examined, with the argument y replacing x in the above expressions. Applying these limits to the factors f_i gives

$$f_1 \rightarrow -ik \frac{\alpha^2}{\omega^2} Y_\alpha, \quad f_2 \rightarrow \left(\frac{\omega^2}{\beta^2} - 2k^2\right) \frac{\alpha^2}{\omega^2} Y_\alpha,$$

$$f_3 \rightarrow \frac{\alpha^2}{\beta^2} Y_\beta, \quad f_4 \rightarrow 2ik \frac{\alpha^2}{\omega^2} Y_\beta, \quad f_5 \rightarrow -\frac{\alpha^2}{\omega^2} Y_\beta,$$

where Y_c (with $c = \alpha$ or $c = \beta$) is defined as

$$Y_c = \begin{cases} -i \frac{\pi}{2} \operatorname{sgn}(\omega), & (\omega/c)^2 - k^2 > 0 \\ 1, & (\omega/c)^2 - k^2 < 0 \end{cases}.$$

Obviously, Y_c can be rewritten as

$$Y_c = \left(\frac{1 + \varepsilon_c}{2}\right) \left[-i \frac{\pi}{2} \operatorname{sgn}(\omega)\right] + \left(\frac{1 - \varepsilon_c}{2}\right).$$

The limiting forms as $a \rightarrow 0$ of the three zeroth-order coefficients A_0 , C_0 , and E_0 required for axisymmetric particle displacement solutions can now be obtained. The above limits for the factors f_i are utilized, together with the stress-volume and stress-area scalars M_r , M_θ , and F_z defined in the text. Applying these limits to the formulae for the coefficients yields

$$A_0 \rightarrow \frac{1}{2\pi\rho\omega^2} \operatorname{sinc}\left(\frac{hk}{2\pi}\right) \left[M_r W_r \left(2k^2 - \frac{\omega^2}{\beta^2}\right) - F_z W_z ik \right] Y_\alpha,$$

$$E_0 \rightarrow \frac{1}{2\pi\rho\beta^2} \operatorname{sinc}\left(\frac{hk}{2\pi}\right) [M_\theta W_\theta] Y_\beta,$$

$$C_0 \rightarrow \frac{1}{2\pi\rho\omega^2} \operatorname{sinc}\left(\frac{hk}{2\pi}\right) [2M_r W_r ik + F_z W_z] Y_\beta.$$

8.4 APPENDIX D: EVALUATION OF A TWO-DIMENSIONAL FOURIER TRANSFORM

Consider the function

$$f(r, z, t) = \frac{1}{\sqrt{r^2 + z^2}} w\left(t - \frac{\sqrt{r^2 + z^2}}{c}\right),$$

where $w(t)$ is an arbitrary function of time t , and c is a wavespeed. The two-dimensional Fourier transform of $f(r, z, t)$ with respect to the variables z and t is defined as

$$F(r, k, \omega) = \int_{-\infty-\infty}^{+\infty+\infty} \int f(r, z, t) \exp[-i(kz + \omega t)] dz dt.$$

The transform over the time variable t may be performed immediately, yielding

$$F(r, k, \omega) = W(\omega) \int_{-\infty}^{+\infty} \frac{1}{\sqrt{r^2 + z^2}} \exp\left[-i\frac{\omega}{c}\sqrt{r^2 + z^2}\right] \exp[-ikz] dz,$$

where $W(\omega)$ is the one-dimensional Fourier transform of $w(t)$. Expanding the two complex exponentials in terms of cosine and sine functions, and exploiting the even and odd symmetries of these trigonometric functions, gives the expression

$$F(r, k, \omega) = 2W(\omega) \left\{ \int_0^{+\infty} \frac{\cos\left(\frac{|\omega|}{c}\sqrt{r^2 + z^2}\right) \cos(|k|z)}{\sqrt{r^2 + z^2}} dz - i \operatorname{sgn}(\omega) \int_0^{+\infty} \frac{\sin\left(\frac{|\omega|}{c}\sqrt{r^2 + z^2}\right) \cos(|k|z)}{\sqrt{r^2 + z^2}} dz \right\}$$

where $\operatorname{sgn}(x)$ is the sign function. These integrals are evaluated with the aid of formulae 3.876 (items 1 and 2) on pages 507-508 in Gradshteyn and Ryzhik (1994). Thus, for $r > 0$ and $|\omega|/c > |k| > 0$:

$$F(r, k, \omega) = 2W(\omega) \left\{ \left[-\frac{\pi}{2} N_0\left(r\sqrt{\frac{\omega^2}{c^2} - k^2}\right) \right] - i \operatorname{sgn}(\omega) \left[\frac{\pi}{2} J_0\left(r\sqrt{\frac{\omega^2}{c^2} - k^2}\right) \right] \right\},$$

where $J_0(x)$ and $N_0(x)$ are Bessel and Neumann functions of order zero, respectively. For $r > 0$ and $|k| > |\omega|/c > 0$:

$$F(r, k, \omega) = 2W(\omega) K_0\left(r\sqrt{k^2 - \frac{\omega^2}{c^2}}\right),$$

where $K_0(x)$ is the modified Bessel function of the third kind, of zero order. $K_0(x)$ is also known as the zeroth-order Basset function or Macdonald function. The above two equations are easily consolidated into a single expression. Define the quantities

$$k_c \equiv \sqrt{\left| \frac{\omega^2}{c^2} - k^2 \right|}, \quad \varepsilon_c \equiv \operatorname{sgn}\left(\frac{\omega^2}{c^2} - k^2\right),$$

and

$$R_0(x) \equiv \begin{cases} J_0(x) - i \operatorname{sgn}(\omega) N_0(x), & \varepsilon_c = +1 \\ K_0(x), & \varepsilon_c = -1 \end{cases}.$$

Then, the two-dimensional Fourier transform becomes

$$F(r, k, \omega) = 2W(\omega)R_0(k_c r) \left\{ \left(\frac{1 + \varepsilon_c}{2} \right) \left[-i \frac{\pi}{2} \operatorname{sgn}(\omega) \right] + \left(\frac{1 - \varepsilon_c}{2} \right) \right\}.$$

Finally, defining

$$Y_c \equiv \left(\frac{1 + \varepsilon_c}{2} \right) \left[-i \frac{\pi}{2} \operatorname{sgn}(\omega) \right] + \left(\frac{1 - \varepsilon_c}{2} \right) = \begin{cases} -i \frac{\pi}{2} \operatorname{sgn}(\omega), & \varepsilon_c = +1 \\ 1, & \varepsilon_c = -1 \end{cases}$$

yields the two-dimensional Fourier transform formula utilized in the text:

$$F(r, k, \omega) = 2W(\omega)R_0(k_c r)Y_c.$$

$F(r, k, \omega)$ is demonstrated to be the forward two-dimensional Fourier transform of $f(r, z, t)$. Then, by Lerch's theorem, $f(r, z, t)$ differs from the inverse two-dimensional Fourier transform of $F(r, k, \omega)$ by at most a null function of the variables z and t .

The definite integral

$$I(r, t; c) \equiv \int_{-\infty}^{+\infty} f(r, z, t) dz$$

is needed for calculating the elastic wavefield radiated from an infinite-length line source. However, this is just the one-dimensional inverse Fourier transform of $F(r, 0, \omega)$:

$$I(r, t; c) = \frac{1}{2\pi} \int_{-\infty}^{+\infty} F(r, 0, \omega) \exp(+i\omega t) d\omega.$$

Evaluating $F(r, k, \omega)$ at wavenumber $k = 0$ gives

$$F(r, 0, \omega) = -\pi W(\omega) \left[N_0\left(\frac{r|\omega|}{c}\right) + i \operatorname{sgn}(\omega) J_0\left(\frac{r|\omega|}{c}\right) \right].$$

Substituting $F(r,0,\omega)$ into the one-dimensional Fourier inversion integral, and exploiting the symmetry properties of the integrand, gives the temporal convolution $I(r,t;c) = w(t)*g(r,t;c)$, where

$$g(r,t;c) = \int_0^{+\infty} \left[J_0\left(\frac{\omega r}{c}\right) \sin(\omega t) - N_0\left(\frac{\omega r}{c}\right) \cos(\omega t) \right] d\omega.$$

The above integrals are evaluated with formulae 6.671 (items 1 and 4) on page 750 of Gradshteyn and Ryzhik (1994), yielding

$$I(r,t;c) = 2w(t)* \left[\frac{H\left(t - \frac{r}{c}\right)}{\sqrt{t^2 - \frac{r^2}{c^2}}} \right],$$

where $H(t)$ is the Heaviside unit step function. The partial derivative of $I(r,t;c)$ with respect to the radius r is also required for calculating infinite line source responses. From the above expression

$$\frac{\partial I(r,t;c)}{\partial r} = \frac{2r}{c^2} w(t)* \left[\frac{H\left(t - \frac{r}{c}\right)}{\left(t^2 - \frac{r^2}{c^2}\right)^{3/2}} \right].$$

However, in order to avoid convergence problems with various convolution integrals, this derivative is written in the equivalent form

$$\frac{\partial I(r,t;c)}{\partial r} = -\frac{2}{r} w'(t)* \left[\frac{tH\left(t - \frac{r}{c}\right)}{\sqrt{t^2 - \frac{r^2}{c^2}}} \right],$$

where the theorem $f(x)*g'(x) = f'(x)*g(x)$ is used.

8.5 APPENDIX E: PARTIAL DERIVATIVES

Several partial derivatives of the function

$$f(r, z, t) = \frac{1}{\sqrt{r^2 + z^2}} w\left(t - \frac{\sqrt{r^2 + z^2}}{c}\right)$$

are required for the analysis. In cylindrical coordinates (r, z) the first-order derivatives are

$$\frac{\partial f}{\partial r} = -\frac{rw'(t - \tau_c)}{c(r^2 + z^2)} - \frac{rw(t - \tau_c)}{(r^2 + z^2)^{3/2}}, \quad \frac{\partial f}{\partial z} = -\frac{zw'(t - \tau_c)}{c(r^2 + z^2)} - \frac{zw(t - \tau_c)}{(r^2 + z^2)^{3/2}}.$$

Three second-order partial derivatives utilized are

$$\frac{\partial^2 f}{\partial r^2} = \frac{r^2 w''(t - \tau_c)}{c^2(r^2 + z^2)^{3/2}} + \frac{(2r^2 - z^2)w'(t - \tau_c)}{c(r^2 + z^2)^2} + \frac{(2r^2 - z^2)w(t - \tau_c)}{(r^2 + z^2)^{5/2}},$$

$$\frac{\partial^2 f}{\partial r \partial z} = \frac{rzw''(t - \tau_c)}{c^2(r^2 + z^2)^{3/2}} + \frac{3rzw'(t - \tau_c)}{c(r^2 + z^2)^2} + \frac{3rzw(t - \tau_c)}{(r^2 + z^2)^{5/2}},$$

$$\frac{\partial^2 f}{\partial z^2} = \frac{z^2 w''(t - \tau_c)}{c^2(r^2 + z^2)^{3/2}} + \frac{(2z^2 - r^2)w'(t - \tau_c)}{c(r^2 + z^2)^2} + \frac{(2z^2 - r^2)w(t - \tau_c)}{(r^2 + z^2)^{5/2}}.$$

Finally, the two third-order partial derivatives needed are

$$\frac{\partial^3 f}{\partial r \partial z^2} = \frac{rz^2 w'''(t - \tau_c)}{c^3(r^2 + z^2)^2} - \frac{r(5z^2 - r^2)w''(t - \tau_c)}{c^2(r^2 + z^2)^{5/2}} - \frac{3r(4z^2 - r^2)w'(t - \tau_c)}{c(r^2 + z^2)^3} - \frac{3r(4z^2 - r^2)w(t - \tau_c)}{(r^2 + z^2)^{7/2}},$$

$$\frac{\partial^3 f}{\partial z^3} = -\frac{z^3 w'''(t - \tau_c)}{c^3(r^2 + z^2)^2} - \frac{3z(z^2 - r^2)w''(t - \tau_c)}{c^2(r^2 + z^2)^{5/2}} - \frac{3z(2z^2 - 3r^2)w'(t - \tau_c)}{c(r^2 + z^2)^3} - \frac{3z(2z^2 - 3r^2)w(t - \tau_c)}{(r^2 + z^2)^{7/2}}.$$

In these expressions, c is a wavespeed, $w(t)$ is a differentiable function of time, and $\tau_c = (1/c) \sqrt{(r^2+z^2)}$ is the propagation time of a wave from the origin to field point (r,z) . It is easily established that $f(r,z,t)$ satisfies the homogeneous three-dimensional scalar wave equation

$$\nabla^2 f - \frac{1}{c^2} \frac{\partial^2 f}{\partial t^2} = 0,$$

where $\nabla^2 = \partial^2/\partial r^2 + (1/r)\partial/\partial r + \partial^2/\partial z^2$ is the axially symmetric Laplacian operator in cylindrical coordinates. Converting the above expressions to spherical polar coordinates via $r = R \sin\varphi$, $z = R \cos\varphi$, and $r^2 + z^2 = R^2$ gives

$$\frac{\partial f}{\partial r} = -\frac{\sin\varphi}{R} \left[\frac{w'(t-\tau_c)}{c} + \frac{w(t-\tau_c)}{R} \right], \quad \frac{\partial f}{\partial z} = -\frac{\cos\varphi}{R} \left[\frac{w'(t-\tau_c)}{c} + \frac{w(t-\tau_c)}{R} \right],$$

$$\frac{\partial^2 f}{\partial r^2} = \frac{1}{R} \left[\frac{\sin^2\varphi w''(t-\tau_c)}{c^2} + \frac{(2-3\cos^2\varphi)w'(t-\tau_c)}{cR} + \frac{(2-3\cos^2\varphi)w(t-\tau_c)}{R^2} \right],$$

$$\frac{\partial^2 f}{\partial r \partial z} = \frac{\sin\varphi \cos\varphi}{R} \left[\frac{w''(t-\tau_c)}{c^2} + \frac{3w'(t-\tau_c)}{cR} + \frac{3w(t-\tau_c)}{R^2} \right],$$

$$\frac{\partial^2 f}{\partial z^2} = \frac{1}{R} \left[\frac{\cos^2\varphi w''(t-\tau_c)}{c^2} + \frac{(3\cos^2\varphi-1)w'(t-\tau_c)}{cR} + \frac{(3\cos^2\varphi-1)w(t-\tau_c)}{R^2} \right],$$

$$\begin{aligned} \frac{\partial^3 f}{\partial r \partial z^2} = \frac{-\sin\varphi}{R} & \left[\frac{\cos^2\varphi w'''(t-\tau_c)}{c^3} + \frac{(6\cos^2\varphi-1)w''(t-\tau_c)}{c^2 R} \right. \\ & \left. + \frac{3(5\cos^2\varphi-1)w'(t-\tau_c)}{cR^2} + \frac{3(5\cos^2\varphi-1)w(t-\tau_c)}{R^3} \right], \end{aligned}$$

$$\begin{aligned} \frac{\partial^3 f}{\partial z^3} = \frac{-\cos\varphi}{R} & \left[\frac{\cos^2\varphi w'''(t-\tau_c)}{c^3} + \frac{3(2\cos^2\varphi-1)w''(t-\tau_c)}{c^2 R} \right. \\ & \left. + \frac{3(5\cos^2\varphi-3)w'(t-\tau_c)}{cR^2} + \frac{3(5\cos^2\varphi-3)w(t-\tau_c)}{R^3} \right], \end{aligned}$$

where the traveltime τ_c now equals R/c .

There are no obvious general formulae for the high-order (i.e., $n > 3$) partial derivatives. However, far-field approximations are readily obtained by retaining only terms proportional to $1/R$. A progression is easily recognized in the above expressions, yielding the far-field approximations

$$\frac{\partial^n f}{\partial z^n} \approx \frac{1}{R} \left(\frac{-\cos \varphi}{c} \right)^n w^{(n)}(t - \tau_c),$$

and

$$\frac{\partial^{n+1} f}{\partial r \partial z^n} \approx \left(\frac{-\sin \varphi}{cR} \right) \left(\frac{-\cos \varphi}{c} \right)^n w^{(n+1)}(t - \tau_c),$$

where $w^{(n)}(t)$ denotes the n^{th} -order derivative of $w(t)$ with respect to its argument.

8.6 APPENDIX F: DIRECTION-DEPENDENT WAVELET

The infinite sum

$$\sum_{n=0}^{\infty} \frac{1}{(2n+1)!} \left(\frac{h \cos \varphi}{2c} \right)^{2n} w^{(2n)}(t)$$

arises repeatedly in the derivation of far-field approximations for the elastic wavefields radiated by various line sources of length h . $w^{(n)}(t)$ denotes the n^{th} -order derivative of the source wavelet $w(t)$ with respect to its argument, and c is a wavespeed (either the compressional wavespeed α or the shear wavespeed β). Fourier transforming on the time variable t yields

$$W(\omega) \sum_{n=0}^{\infty} \frac{1}{(2n+1)!} \left[- \left(\frac{\omega h \cos \varphi}{2c} \right)^2 \right]^n.$$

The infinite sum is a power series representation of the function $\text{sinc}(x) \equiv \sin(\pi x)/(\pi x)$, evaluated at argument $x = \omega h \cos \varphi / 2\pi c$. Hence

$$W(\omega) \sum_{n=0}^{\infty} \frac{1}{(2n+1)!} \left[- \left(\frac{\omega h \cos \varphi}{2c} \right)^2 \right]^n = W(\omega) \text{sinc} \left(\frac{\omega h \cos \varphi}{2\pi c} \right).$$

Inverse Fourier transforming back to the time-domain gives

$$\sum_{n=0}^{\infty} \frac{1}{(2n+1)!} \left(\frac{h \cos \varphi}{2c} \right)^{2n} w^{(2n)}(t) = \frac{1}{t_c(\varphi)} \Pi \left(\frac{t}{t_c(\varphi)} \right) * w(t),$$

where $\Pi(x)$ is the rectangle function of unit height and area, and $t_c(\varphi) = h|\cos \varphi|/c$. Defining a *direction-dependent source wavelet* as

$$w(t, \varphi) \equiv \frac{1}{t_c(\varphi)} \Pi \left(\frac{t}{t_c(\varphi)} \right) * w(t),$$

yields the following compact expression for the infinite series:

$$\sum_{n=0}^{\infty} \frac{1}{(2n+1)!} \left(\frac{h \cos \varphi}{2c} \right)^{2n} w^{(2n)}(t) = w(t, \varphi).$$

Symbolically, the direction-dependent waveform $w(t, \varphi)$ is distinguished from the isotropic wavelet $w(t)$ via two arguments, rather than one.

Note that the direction-dependent source wavelet is a moving average of the physical source wavelet over a time window of duration $t_c(\varphi)$:

$$w(t, \varphi) = \frac{1}{t_c(\varphi)} \int_{t-t_c(\varphi)/2}^{t+t_c(\varphi)/2} w(\tau) d\tau.$$

The length of the time window depends on the polar angle φ . As $\varphi \rightarrow \pi/2$, $t_c(\varphi) \rightarrow 0$, and thus $[1/t_c(\varphi)]\Pi[t/t_c(\varphi)]$ approaches a temporal Dirac delta function $\delta(t)$. Hence, $w(t, \pi/2) = w(t)$. In the perpendicular bisector plane to the line source, the direction-dependent wavelet is identical to the physical source wavelet. The averaging window length $t_c(\varphi)$ has a simple geometric interpretation. It is the time required for a plane wave, advancing with speed c in the direction φ , to propagate a distance h parallel to the z -coordinate axis. Alternately, the apparent speed of the plane wave along the z -axis is $h/t_c(\varphi)$.

Finally, some of the far-field elastodynamic wavefields depend on the time derivative of the direction-dependent wavelet. Using the theorem $d/dx[f(x)*g(x)] = f'(x)*g(x) = f(x)*g'(x)$, it is easily established that

$$\frac{\partial w(t, \varphi)}{\partial t} = \frac{1}{t_c(\varphi)} [\delta(t + t_c(\varphi)/2) - \delta(t - t_c(\varphi)/2)] * w(t) = \frac{w(t + t_c(\varphi)/2) - w(t - t_c(\varphi)/2)}{t_c(\varphi)}.$$

Note that $\partial w(t, \pi/2) / \partial t = w'(t)$, as expected.

8.7 APPENDIX G: POINT SOURCE WAVEFIELDS

Expressions for the wavefields radiated from three different point sources located in a homogeneous and isotropic elastic wholespace are tabulated below. The medium is characterized by P-wave speed α , S-wave speed β , and mass density ρ . A spherical polar coordinate system originates at the source point. P-wave and S-wave traveltimes from the origin to radial distance R are $\tau_\alpha = R/\alpha$ and $\tau_\beta = R/\beta$, respectively. Polar angle φ ($0 \leq \varphi \leq \pi$) is measured from the $+z$ -axis. The wavefields are axially symmetric; they exhibit no dependence on the azimuthal angle θ . All source wavelets are given by the dimensionless waveform $w(t)$, which is normalized to unit maximum absolute amplitude. Finally, a prime designates differentiation of a function with respect to its argument.

8.7.1 Unidirectional Torque

The particle displacement generated by a point torque of magnitude M oriented in the $+z$ direction is

$$u_\theta \Big|_{\text{point}} = \left(\frac{M \sin \varphi}{4\pi\rho R} \right) \left[\frac{w'(t - \tau_\beta)}{\beta^3} + \frac{w(t - \tau_\beta)}{\beta^2 R} \right].$$

The displacement propagates outward as an S-wave polarized in horizontal planes (SH motion). No compressional (P) waves or vertically polarized shear (SV) waves are generated. Both far-field (proportional to $1/R$) and near-field (proportional to $1/R^2$) terms exist. The $\sin\varphi$ radiation pattern implies that the displacement vanishes along the axis of the torque ($\varphi = 0$ and $\varphi = \pi$), and is maximum perpendicular to the torque vector ($\varphi = \pi/2$). Since the displacement wavefield is equivoluminal, the pressure radiated from a point torque is identically zero.

8.7.2 Unidirectional Force

The particle acceleration components radiated from a point force of magnitude F oriented in the $+z$ direction are

$$\frac{\partial^2 u_R}{\partial t^2} \Big|_{\text{point}} = \left(\frac{F \cos \varphi}{4\pi\rho R} \right) \left\{ \left[\frac{w''(t - \tau_\alpha)}{\alpha^2} + \frac{2w'(t - \tau_\alpha)}{\alpha R} + \frac{2w(t - \tau_\alpha)}{R^2} \right] - \left[\frac{2w'(t - \tau_\beta)}{\beta R} + \frac{2w(t - \tau_\beta)}{R^2} \right] \right\},$$

$$\frac{\partial^2 u_\varphi}{\partial t^2} \Big|_{\text{point}} = \left(\frac{F \sin \varphi}{4\pi\rho R} \right) \left\{ \left[\frac{w'(t - \tau_\alpha)}{\alpha R} + \frac{w(t - \tau_\alpha)}{R^2} \right] - \left[\frac{w''(t - \tau_\beta)}{\beta^2} + \frac{w'(t - \tau_\beta)}{\beta R} + \frac{w(t - \tau_\beta)}{R^2} \right] \right\}.$$

The equations contain far-field terms (proportional to $1/R$) and near-field terms (proportional to $1/R^2$ and $1/R^3$) for both compressional and shear radiation. Far-field P-waves are longitudinal and far-field S-waves are transverse. Particle displacement waveforms for each are identical to the source force waveform $w(t)$. Radiation patterns for the radial and polar components of motion exhibit cosine and sine dependence on the polar angle φ , respectively. However, it is apparent that this holds for the *entire* wavefield (P and S, near and far) rather than just the far-field P and S portions, respectively. The pressure wavefield radiated from the unidirectional point force is

$$p|_{\text{point}} = \left(\frac{F \cos \varphi}{4\pi R} \right) \left(1 - \frac{4}{3} \gamma^2 \right) \left[\frac{w'(t - \tau_\alpha)}{\alpha} + \frac{w(t - \tau_\alpha)}{R} \right],$$

where $\gamma = \beta/\alpha$. Note that the propagating pressure wavelet changes shape from the near-field to the far-field. In the far-field, it is proportional to the derivative of the source force waveform. Moreover, the pressure wavefield vanishes on the nodal plane defined by $\varphi = \pi/2$.

8.7.3 Ring Pressure

The particle acceleration components radiated from a point pressurized ring source with symmetry axis oriented along the z -coordinate axis are compactly expressed as

$$\frac{\partial^2 u_R}{\partial t^2} \Big|_{\text{point}} = \left(\frac{M}{4\pi\rho R} \right) \left\{ \left(\frac{\alpha^2}{\beta^2} - 2 \cos^2 \varphi \right) \left[\frac{w'''(t - \tau_\alpha)}{\alpha^3} + \frac{w''(t - \tau_\alpha)}{\alpha^2 R} \right] - 2(3 \cos^2 \varphi - 1)q(R, t) \right\},$$

$$\frac{\partial^2 u_\varphi}{\partial t^2} \Big|_{\text{point}} = \left(\frac{M \sin 2\varphi}{4\pi\rho R} \right) \left\{ \left[\frac{w'''(t - \tau_\beta)}{\beta^3} + \frac{w''(t - \tau_\beta)}{\beta^2 R} \right] - 2q(R, t) \right\},$$

where

$$q(R, t) \equiv \frac{w''(t - \tau_\alpha)}{\alpha^2 R} - \frac{w''(t - \tau_\beta)}{\beta^2 R} + \frac{3w'(t - \tau_\alpha)}{\alpha R^2} - \frac{3w'(t - \tau_\beta)}{\beta R^2} + \frac{3w(t - \tau_\alpha) - 3w(t - \tau_\beta)}{R^3}.$$

M is the moment magnitude of the point ring source. Like the unidirectional point force, the ring source simultaneously radiates compressional and shear waves, with motion polarized in vertical (R, φ) planes. Also, far-field (proportional to $1/R$) P-wave and S-wave motions are longitudinal and transverse, respectively. In contrast to the force source, far-field displacement wavelets equal the first derivative of the source waveform, rather the source waveform itself. Near-field terms are proportional to $1/R^n$ where $n = 2, 3$, and 4.

The radiation pattern for radial component motion exhibits some complexities not previously evident. Far-field P-waves have the classic $(\alpha/\beta)^2 - 2\cos^2 \varphi$ angular dependence, first identified by Heelan (1953). Thus, this radiation pattern depends on the medium properties in addition to the polar angle φ . Near-field radial acceleration has a *different* radiation pattern. The radiation pattern for transverse component motion is much simpler: the *entire* transverse wavefield (P and S, near and far) is subject to $\sin 2\varphi$

angular dependence. Hence, SV-waves are strongly beamed at angles $\varphi = \pi/4$ and $\varphi = 3\pi/4$ with respect to the source axis.

Finally, the acoustic pressure wavefield radiated from the ring source is

$$p|_{\text{point}} = \left(\frac{M}{4\pi R} \right) \left(1 - \frac{4}{3} \gamma^2 \right) \left\{ \left(\frac{\alpha^2}{\beta^2} - 2 \cos^2 \varphi \right) \frac{w''(t - \tau_\alpha)}{\alpha^2} + (1 - 3 \cos^2 \varphi) \left[\frac{w'(t - \tau_\alpha)}{\alpha R} + \frac{w(t - \tau_\alpha)}{R^2} \right] \right\}.$$

Thus, the far-field pressure wavelet is proportional to the second derivative of the source waveform. The far-field pressure has the same radiation pattern as the far-field radial acceleration, and there is no nodal plane on which the entire pressure wavefield vanishes.

9.0 FIGURES

Figure 1: Traveltime fields for a line source (heavy contours) and a point source (light contours). Each traveltime function is normalized by h/c and is displayed with a contour interval of 0.5.

Figure 2: The source wavelet $w(t)$ and its frequency amplitude spectrum $|W(\omega)|$ used in the numerical examples. T is the wavelet duration and $\omega_0 = 2\pi/T$ is a characteristic angular frequency. The amplitude spectrum is normalized to unit peak magnitude for plotting purposes.

Figure 3: Response functions of the far-field directional filter $\text{sinc}(\omega \cos \phi / \omega_c)$ that converts a point source wavefield to a line source wavefield. $\omega_c = 2\pi c/h$ is a characteristic angular frequency of the source. Seven curves are plotted corresponding to polar angles $\phi = 0^\circ$ (inline response) to $\phi = 90^\circ$ (broadside response) in increments of 15° . The broadside response equals 1.0 for all dimensionless angular frequencies ω/ω_c .

Figure 4: Far-field radial and transverse particle velocity traces generated by a point force source. Trace length is 150 ms.

Figure 5: Far-field radial and transverse particle velocity traces generated by a point torque source. Trace length is 150 ms.

Figure 6: Far-field radial and transverse particle velocity traces generated by a point ring pressure source. Trace length is 150 ms.

Figure 7: Far-field radial and transverse particle velocity traces generated by a line force source with length $h = 5$ m. Trace length is 150 ms.

Figure 8: Far-field radial and transverse particle velocity traces generated by a line torque source with length $h = 5$ m. Trace length is 150 ms.

Figure 9: Far-field radial and transverse particle velocity traces generated by a line ring pressure source with length $h = 5$ m. Trace length is 150 ms.

Figure 10: Far-field radial and transverse particle velocity traces generated by a line force source with length $h = 10$ m. Trace length is 150 ms.

Figure 11: Far-field radial and transverse particle velocity traces generated by a line torque source with length $h = 10$ m. Trace length is 150 ms.

Figure 12: Far-field radial and transverse particle velocity traces generated by a line ring pressure source with length $h = 10$ m. Trace length is 150 ms.

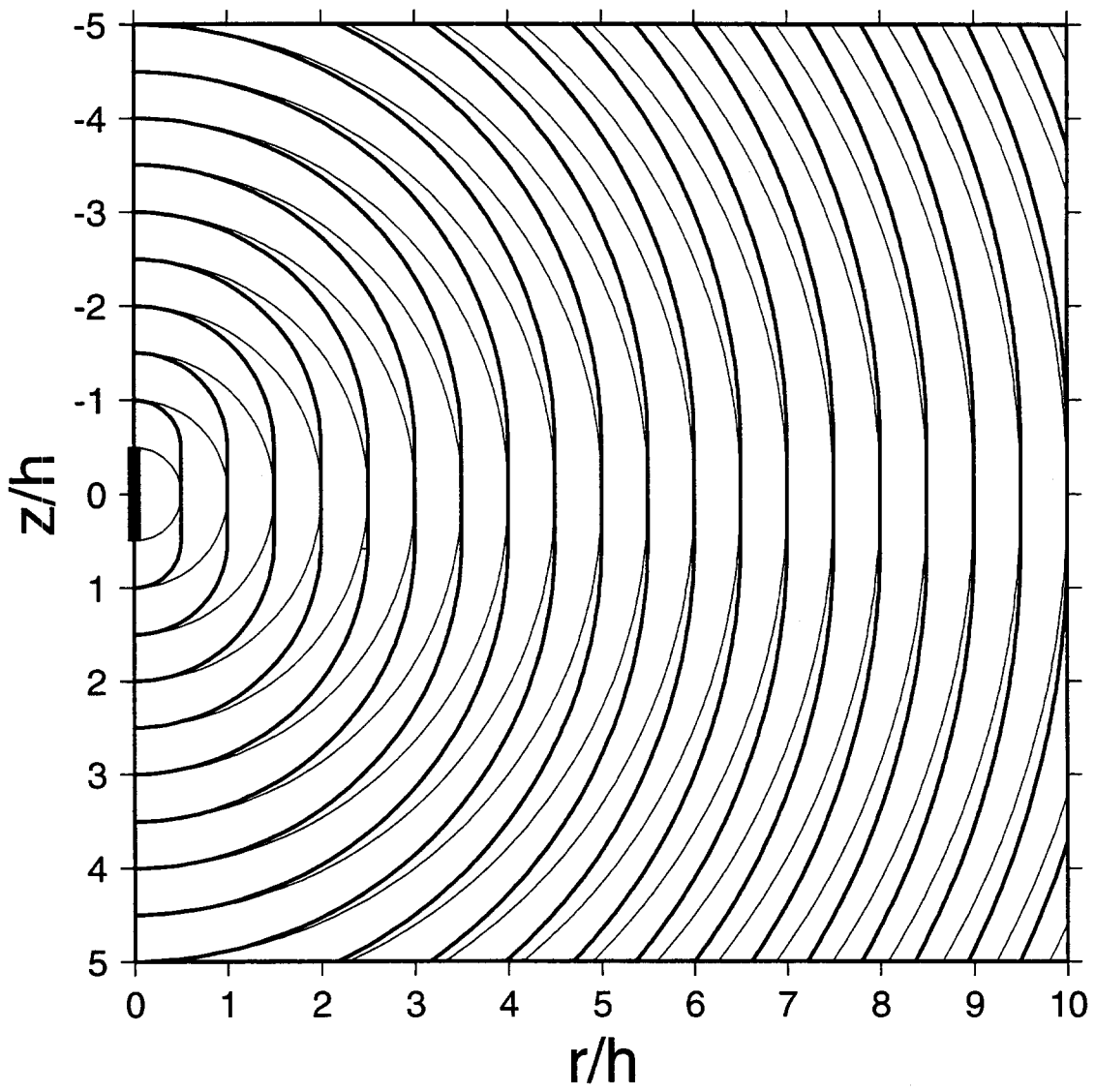


Figure 1

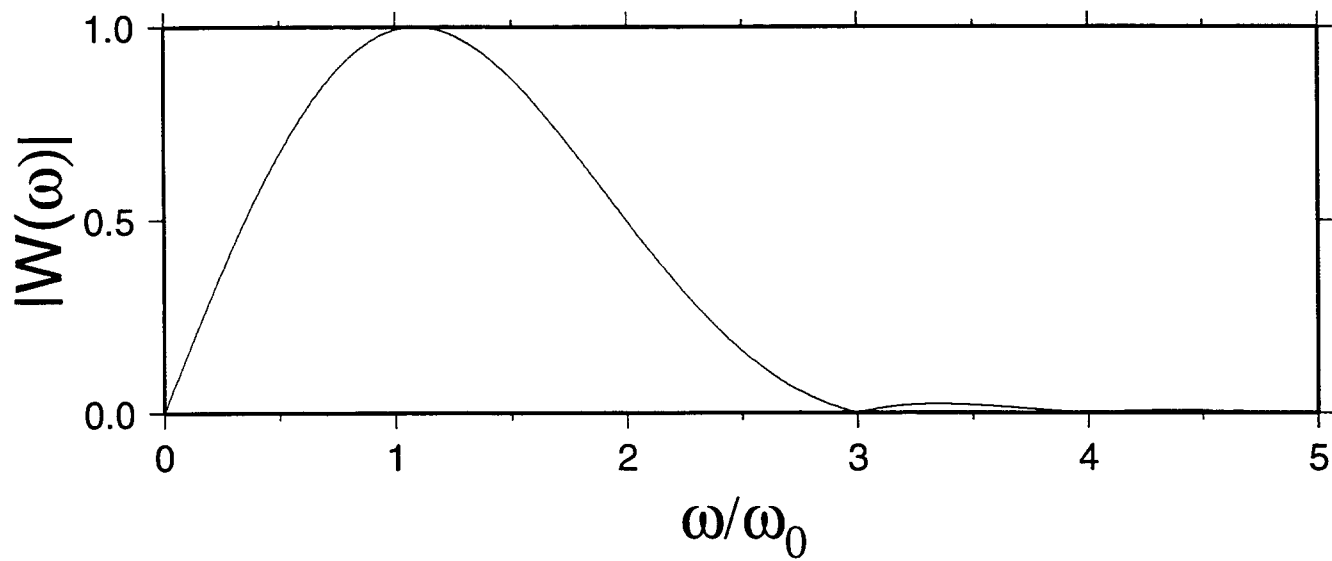
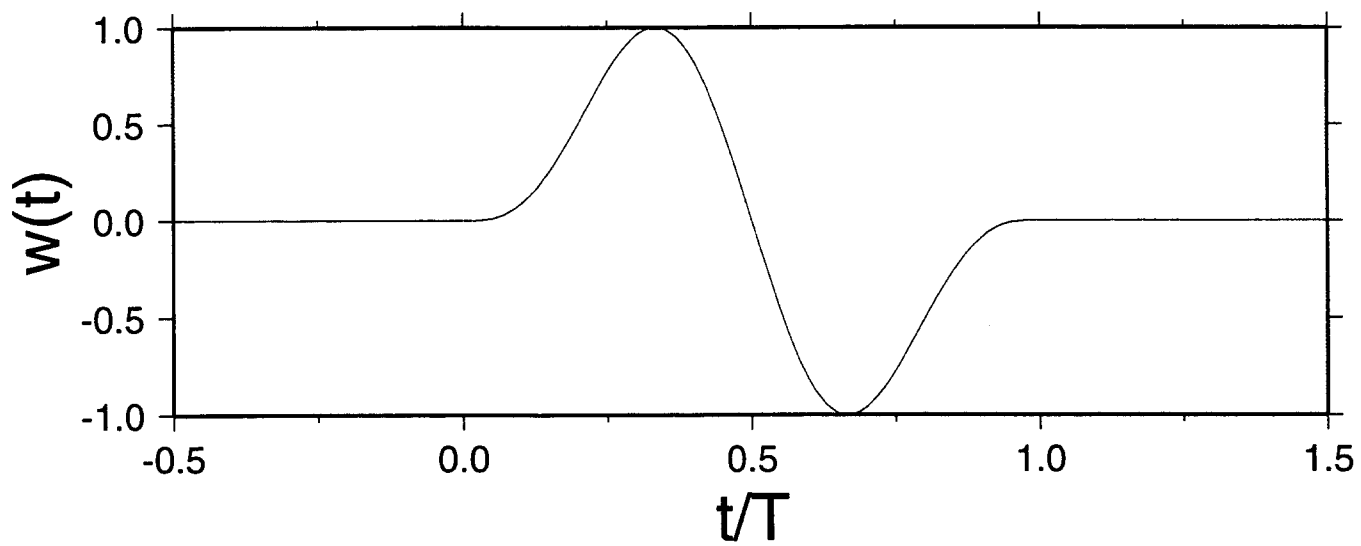


Figure 2

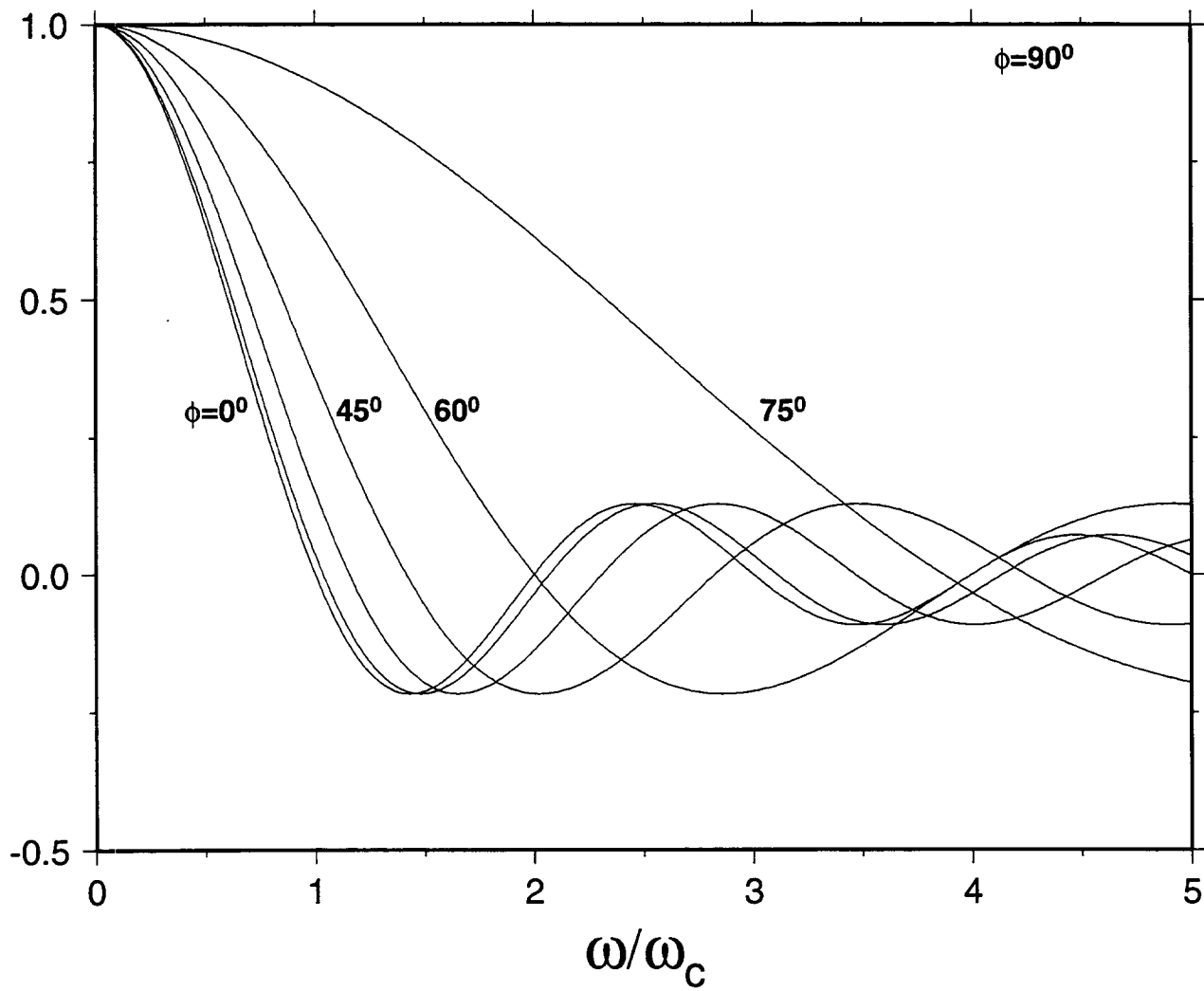


Figure 3

Point Force Source

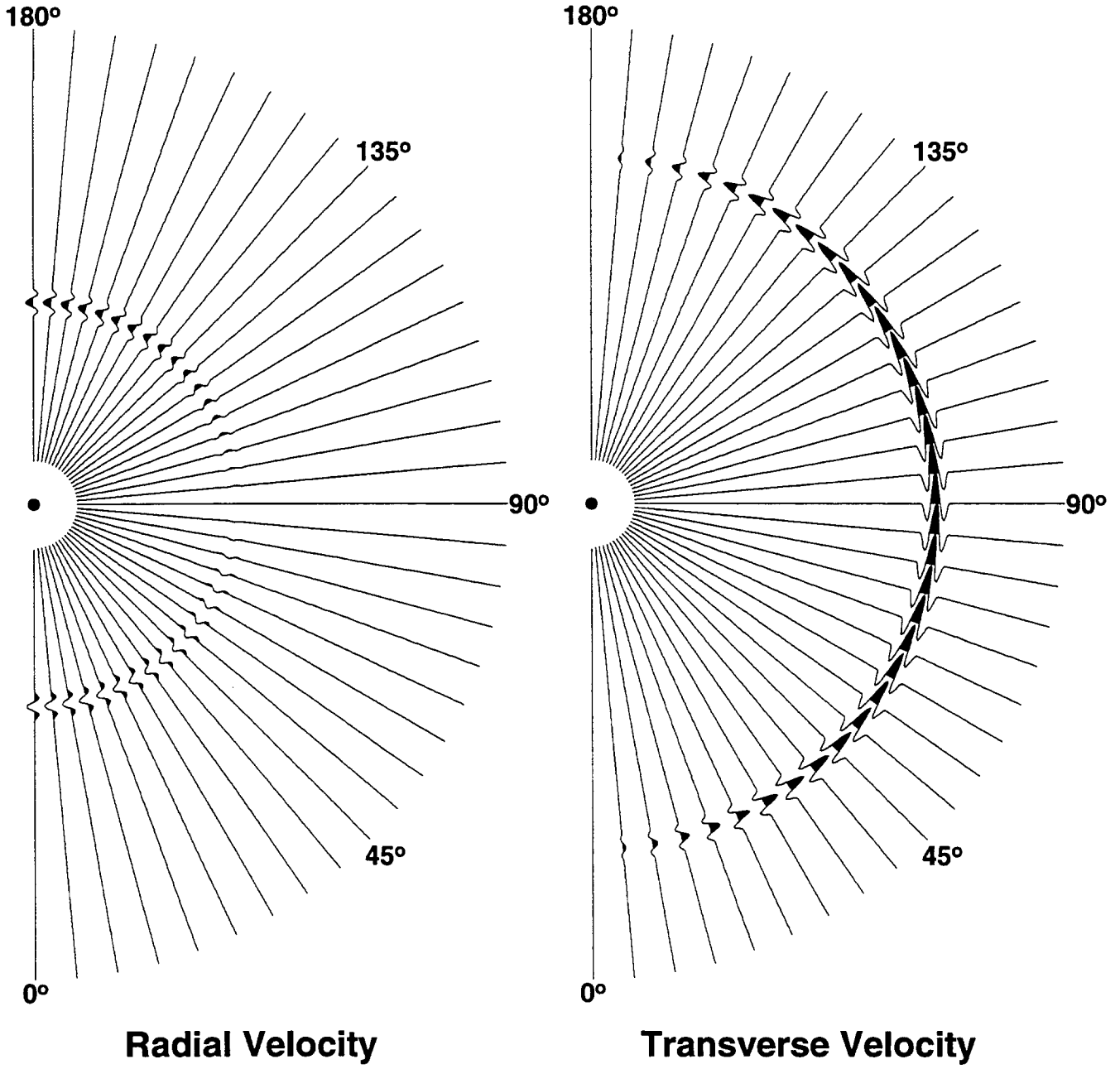


Figure 4

Point Torque Source

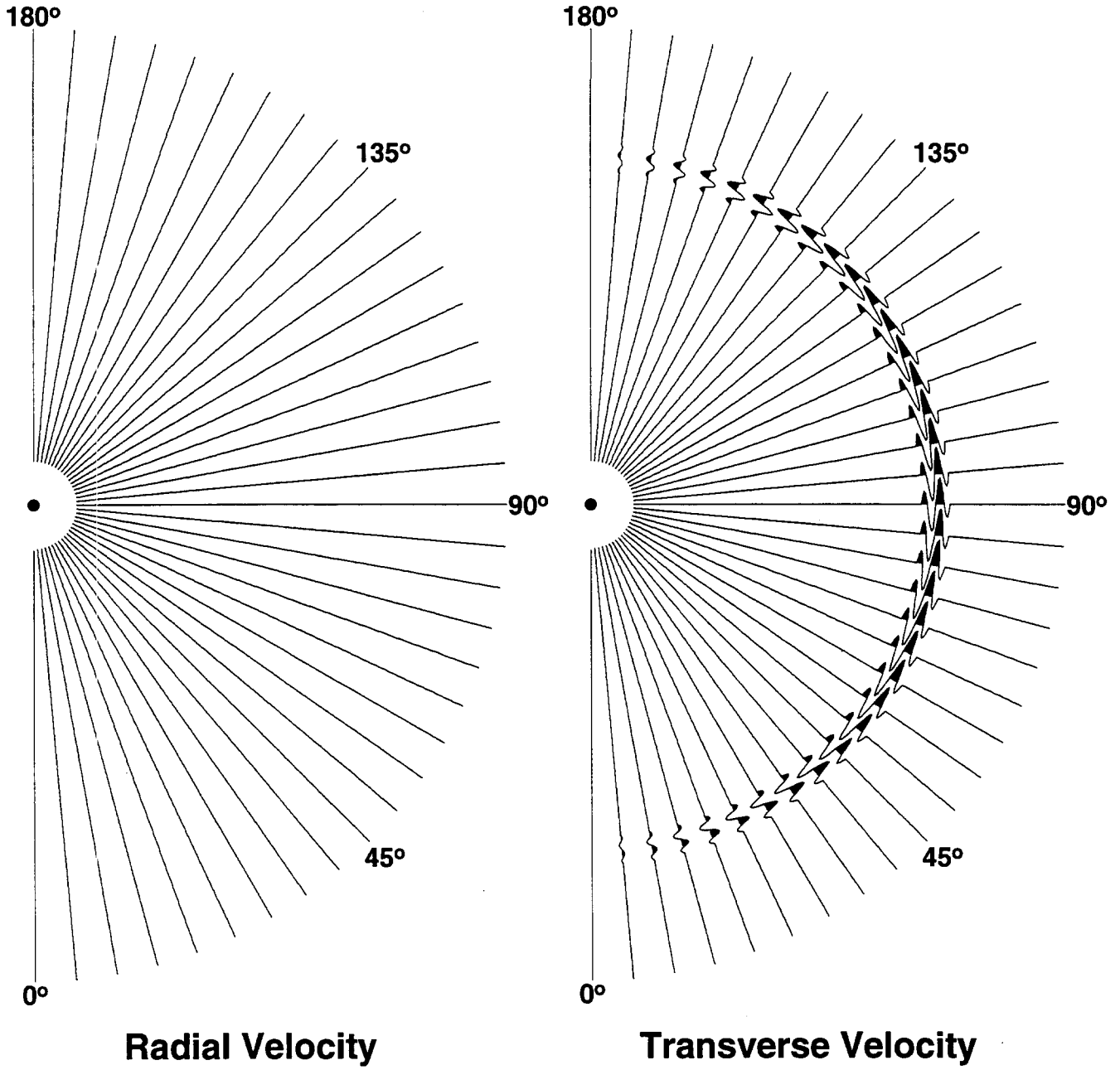


Figure 5

Point Pressure Source

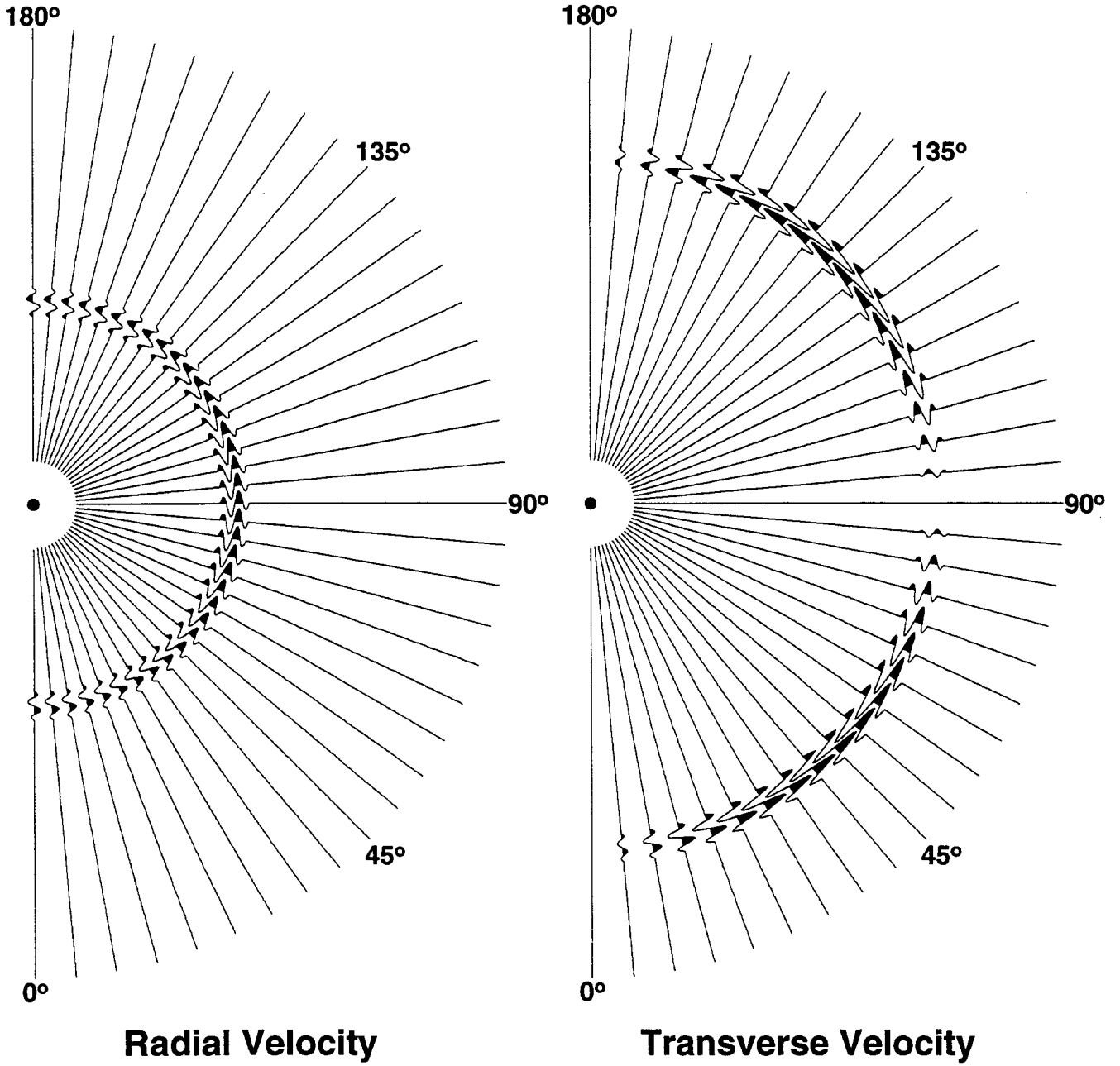


Figure 6

Line Force Source

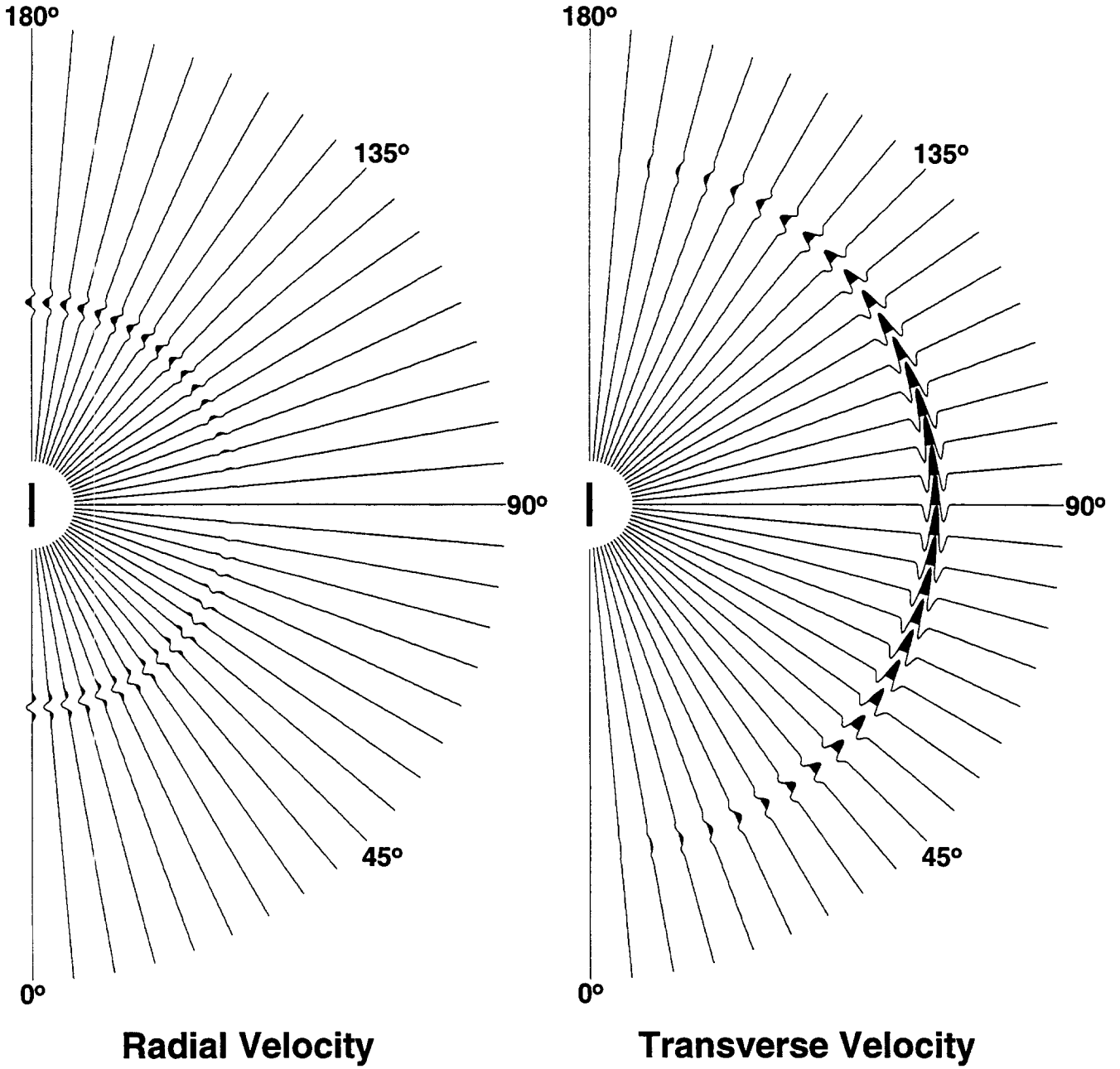


Figure 7

Line Torque Source

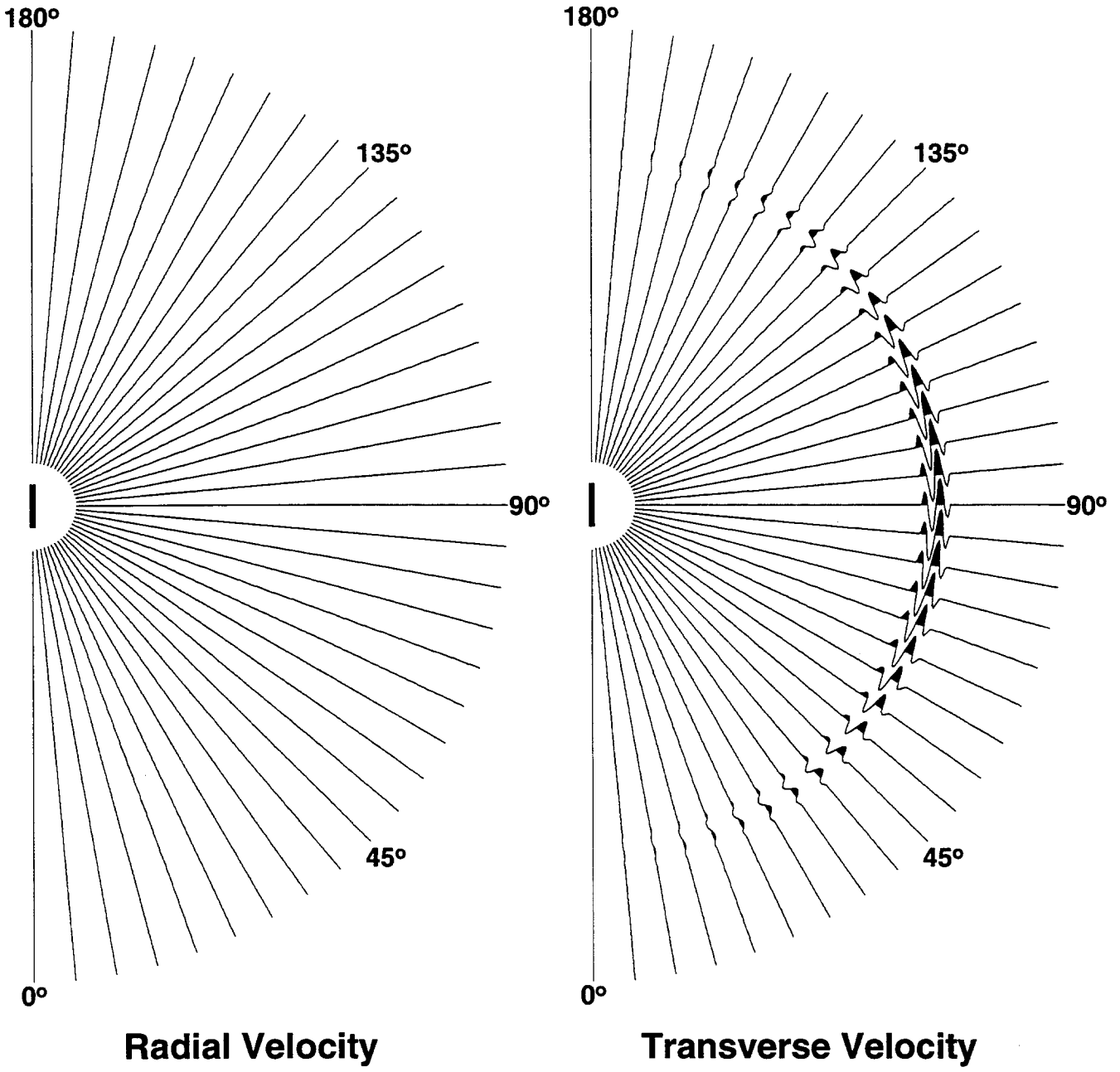


Figure 8

Line Pressure Source

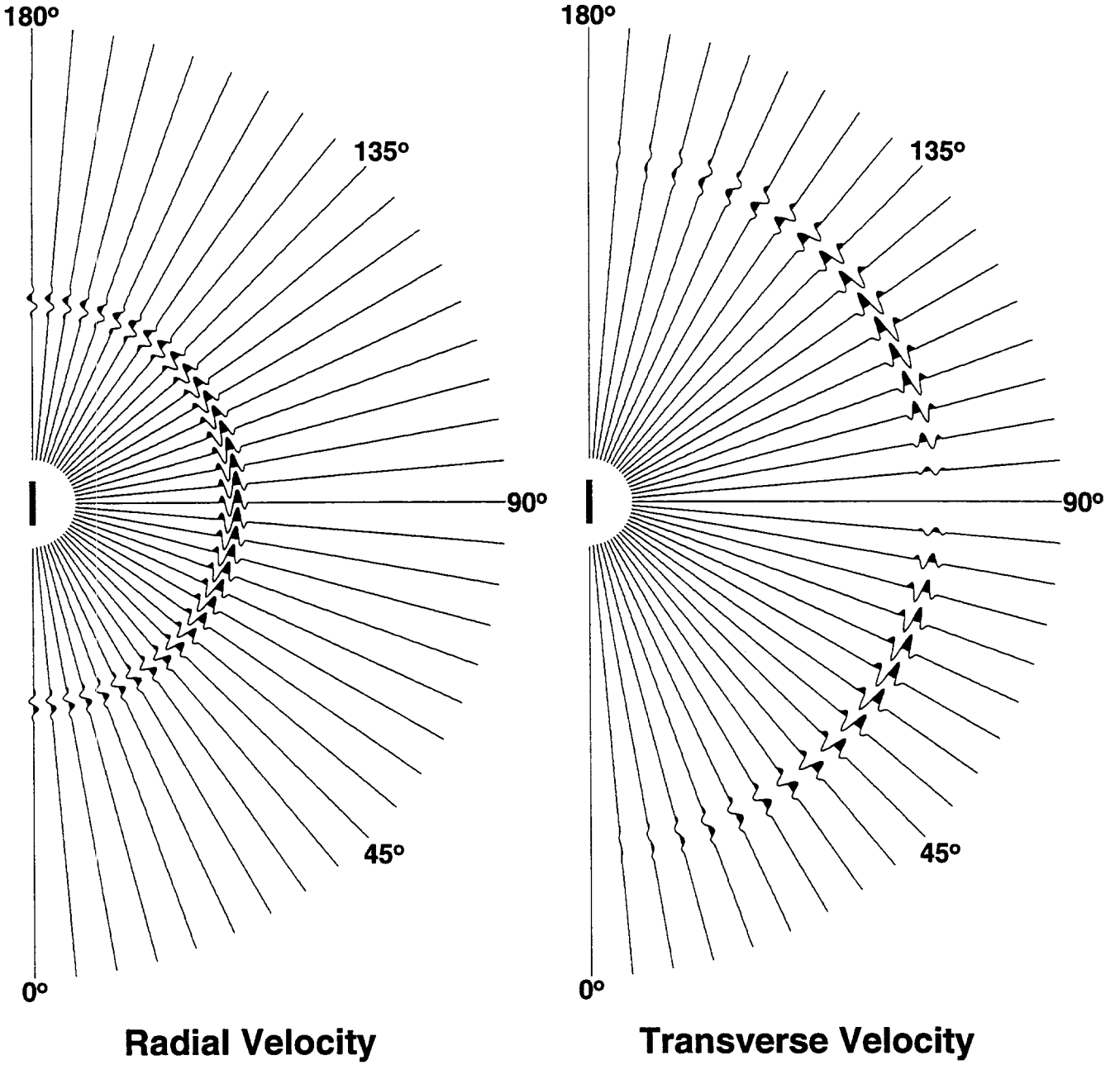


Figure 9

Line Force Source

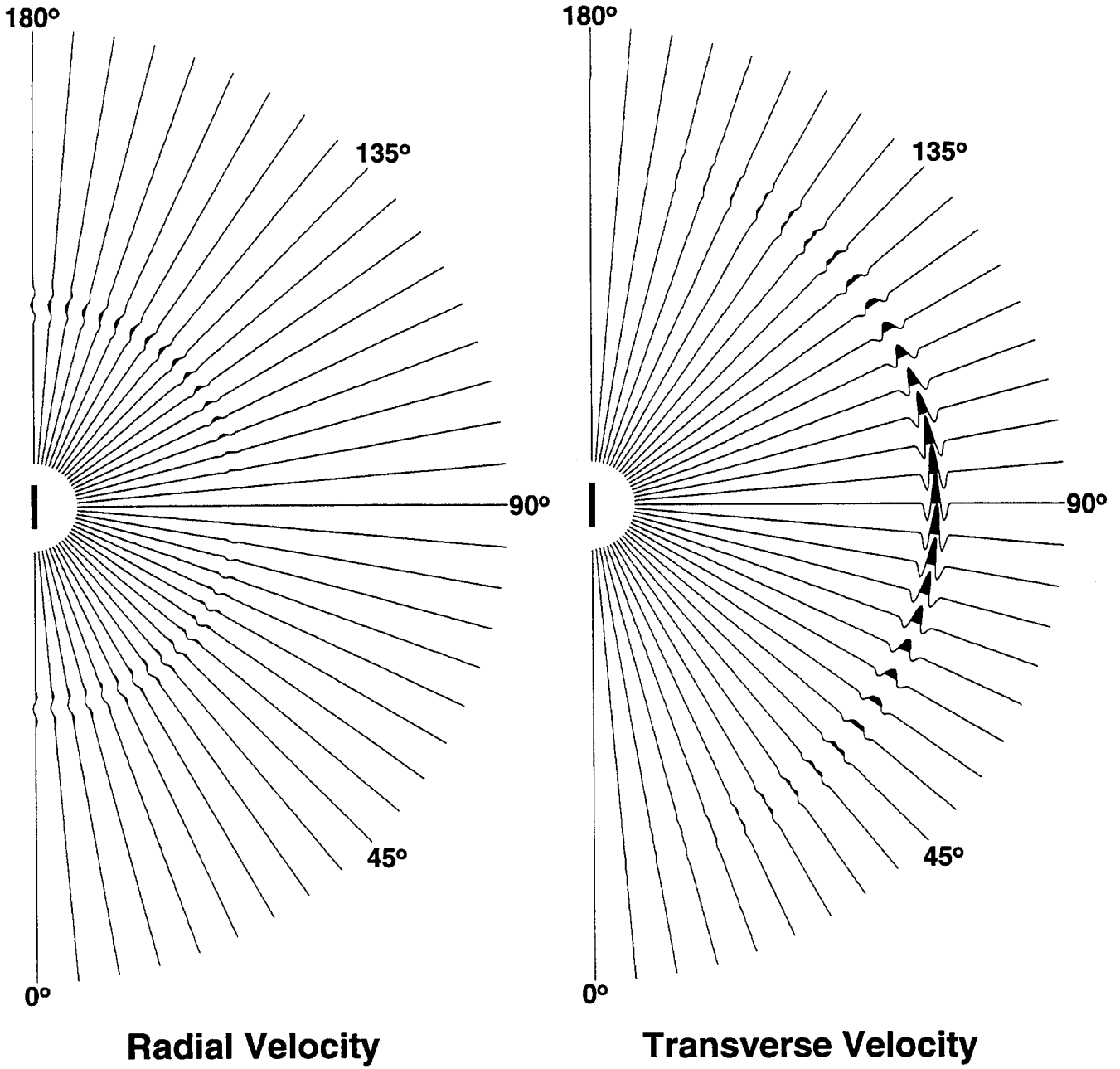


Figure 10

Line Torque Source

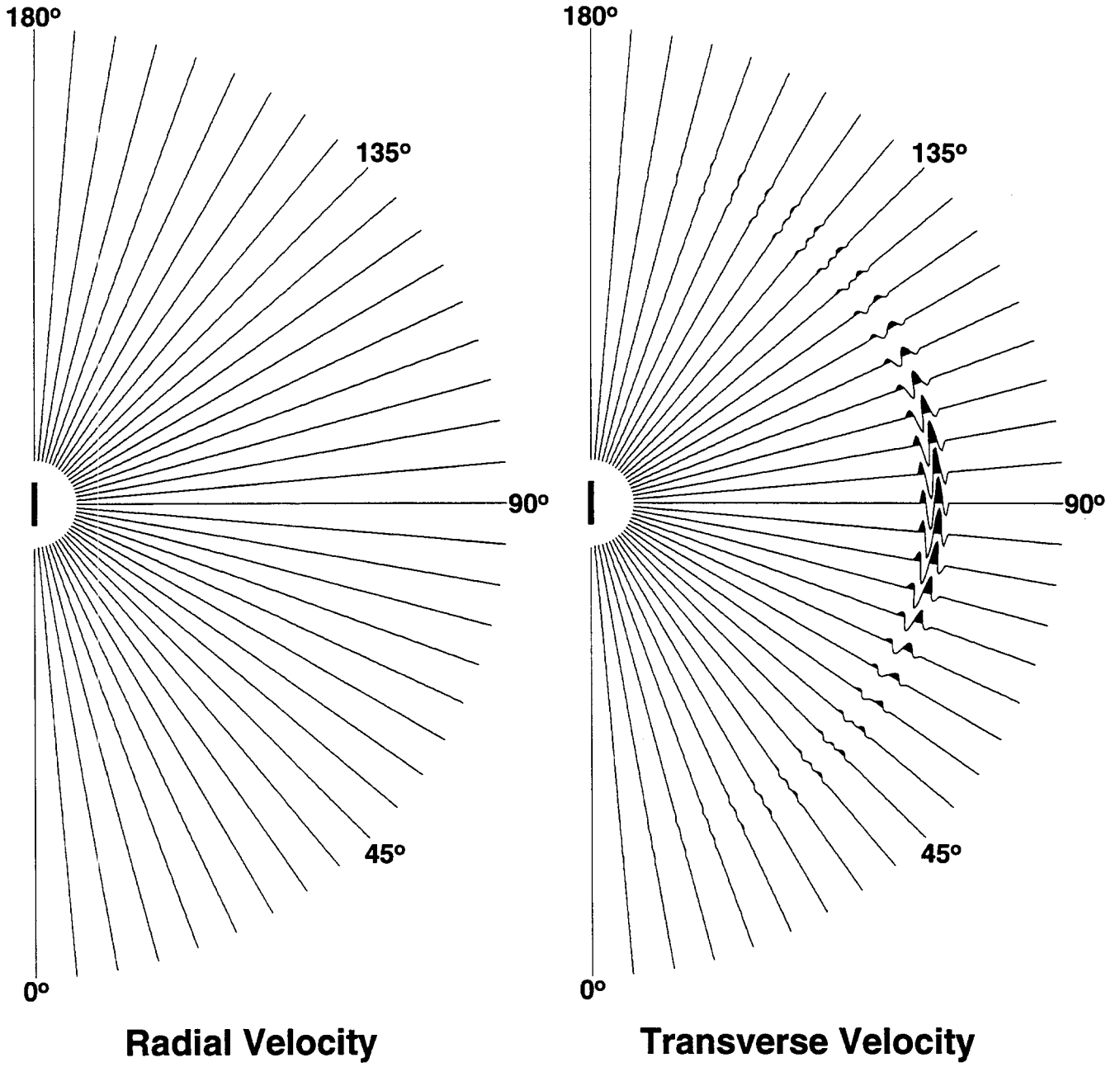


Figure 11

Line Pressure Source

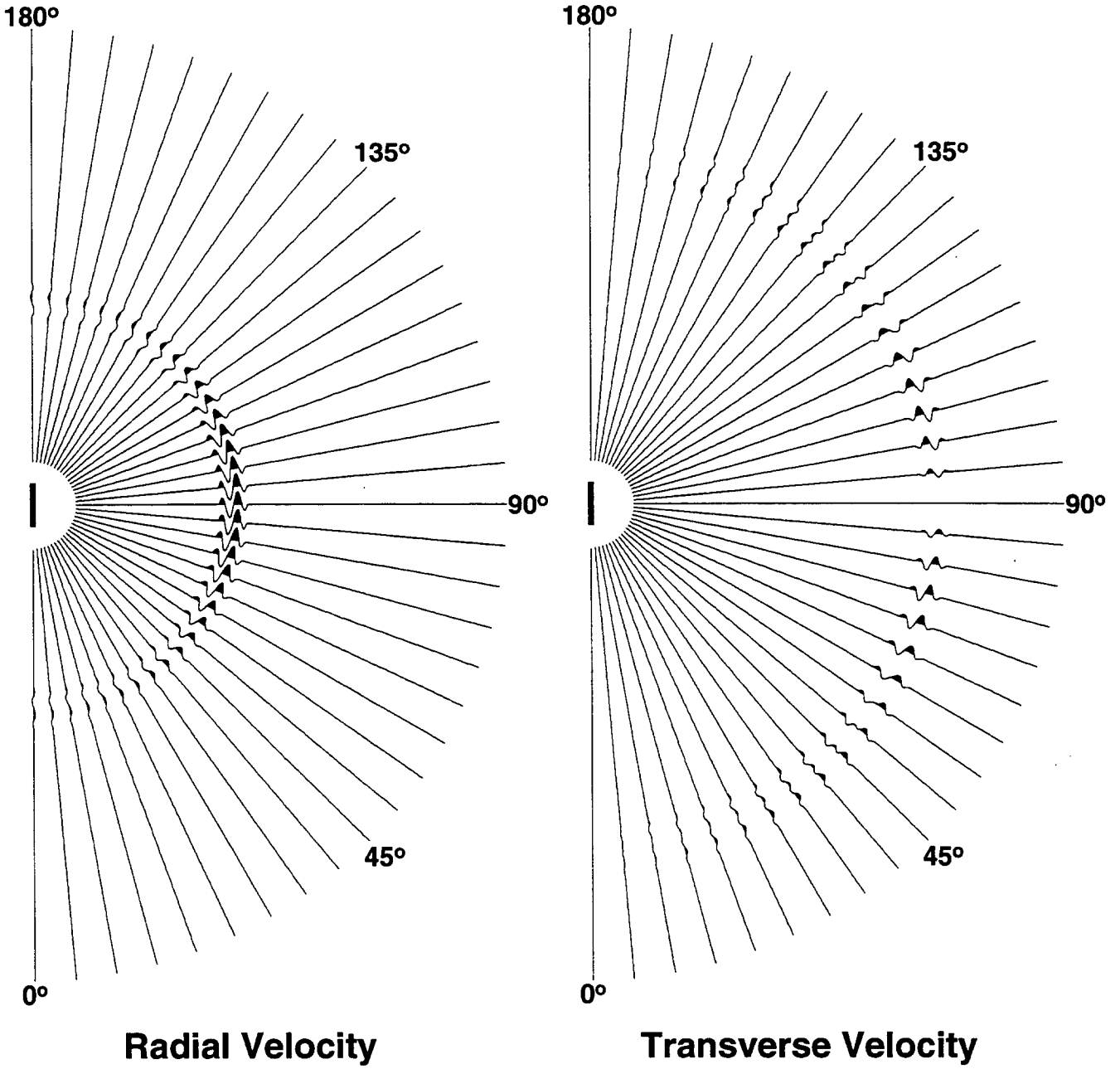


Figure 12

DISTRIBUTION: Sandia National Laboratories Personnel

Organization 2693, Mailstop 0859:

Mark D. Ladd
Gerard E. Sleaf

Organization 5736, Mailstop 0655:

Dorthe B. Carr
Eric P. Chael
John P. Claassen

Organization 6116, Mailstop 0750:

David F. Aldridge (20 copies)
David L. Alumbaugh
Sanford Ballard
Lewis C. Bartel
David J. Borns
Thurlow W.H. Caffey
Gregory J. Elbring
Gregory A. Newman
Neill P. Symons
Marianne C. Walck
Norman R. Warpinski
Christopher J. Young

Organization 9222, Mailstop 1110:

Susan E. Minkoff
David E. Womble

Organization 9234, Mailstop 0439:

Jeffrey L. Dohner

Organization 9321, Mailstop 1168:

H. Douglas Garbin

Technical Library: Organization 4916, Mailstop 0899 (2 copies)

Central Technical Files: Organization 8940-2, Mailstop 9018

**Review and Approval Desk: Organization 15102, Mailstop 0619
For DOE/OSTI**

DISTRIBUTION: Non-SNL Personnel

Ari Ben-Menahem
Weizmann Institute of Science
Rehovot, Israel, 76100

Andrew J. Calvert
Simon Fraser University
Department of Earth Sciences
8888 University Drive
Burnaby, British Columbia, Canada, V5A 1S6

Mark Casady
Vastar Resources
P.O. Box 219276
Houston, Texas, 77079

Thomas Catlett
Spirit Energy 76
4021-4023 Ambassador Caffery Parkway
Lafayette, Louisiana, 70503

Sen T. Chen
Exxon Production Research Company
P.O. Box 2189
Houston, Texas, 77252-2189

Arthur Cheng
Western Atlas Logging Services
P.O. Box 1407
Houston, Texas, 77251-1407

Richard T. Coates
Schlumberger-Doll Research
Old Quarry Road
Ridgefield, Connecticut, 06877

V. Dale Cox
Conoco Incorporated
1000 South Pine
P.O. Box 1267
Ponca City, Oklahoma, 74602-1267

Clifford T. Crowe
Texaco Exploration and Production Incorporated
400 Poydras Street
New Orleans, Louisiana, 70130

Brian N. Fuller
Paulsson Geophysical Services Incorporated
1300 Beach Boulevard
La Habra, California, 90631-6394

Richard L. Gibson, Jr.
Texas A&M University
Department of Geology and Geophysics
College Station, Texas, 77843

Jerry M. Harris
Stanford University
Department of Geophysics
Stanford, California, 94305

Donald V. Helmberger
California Institute of Technology
Seismological Laboratory 252-21
Pasadena, California, 91125

Brian Hornby
Arco Exploration and Production Technology
2300 West Plano Parkway
Plano, Texas, 75075-8499

Donald L. Howlett
Texaco Exploration and Production Technology
3901 Briarpark
Houston, Texas, 77042

John M. Hufford
Phillips Petroleum Incorporated
530H Plaza Office Building
Bartlesville, Oklahoma, 74004

Lane R. Johnson
University of California, Berkeley
Department of Geology and Geophysics
Berkeley, California, 94720

N. Won Kim
Shell Offshore Incorporated
701 Poydras Street
New Orleans, Louisiana, 70139

Robert T. Langan
Chevron Petroleum Technology Company
1300 Beach Boulevard
La Habra, California, 90631-6394

Ernest L. Majer
Lawrence Berkeley National Laboratory
1 Cyclotron Road
Building 90, Mail Stop 1116
Berkeley, California, 94720

Mark A. Meadows
Chevron Petroleum Technology Company
1300 Beach Boulevard
La Habra, California, 90631-6374

Bjorn N.P. Paulsson
Paulsson Geophysical Services Incorporated
1300 Beach Boulevard
La Habra, California, 90631-6394

Jose A. Rial
University of North Carolina
Geology Department
Chapel Hill, North Carolina, 27514

Paul G. Richards
Columbia University
Lamont-Doherty Earth Observatory
Palisades, New York, 10964

Gerard T. Schuster
University of Utah
Department of Geology and Geophysics
Salt Lake City, Utah, 84112

Henry Tan
Amoco Production Company
4502 East 41st Street
P.O. Box 3385
Tulsa, Oklahoma, 74102-3385

M. Nafi Toksoz
Massachusetts Institute of Technology
Earth Resources Laboratory
42 Carleton Street
Cambridge, Massachusetts, 02142

Roger Turpening
Massachusetts Institute of Technology
Earth Resources Laboratory
42 Carleton Street
Cambridge, Massachusetts, 02142

David M. Weinberg
Idaho National Engineering and Environmental Laboratory
P.O. Box 1625
Idaho Falls, Idaho, 83425-2110

Matthew J. Yedlin
University of British Columbia
Department of Geophysics
2219 Main Mall
Vancouver, British Columbia, Canada, V6T 1Z4